



Technical Transfer Dispatch #6

ULSAB-AVC Body Structure Materials

May 2001

FOREWORD

- 1.0 Introduction
- 2.0 Materials Selected for the ULSAB-AVC Body Structure
- 3.0 Advanced High Strength Steel Microstructures, Behavior, and Alloy Design
- 4.0 Materials Selection Process for ULSAB-AVC
- 5.0 Forming Assessment

Appendices:

- I ULSAB-AVC Body Structure Parts List
- II ULSAB-AVC Steel Grades Portfolio
- III Considerations in the Selection of Advanced High Strength Steels for ULSAB-AVC
- IV Examples of ULSAB-AVC Forming Simulations

FOREWORD

Program Background

ULSAB-AVC (Advanced Vehicle Concepts) is the most recent addition to the global steel industry's series of initiatives offering steel solutions to the challenges facing automakers around the world to increase the fuel efficiency of automobiles, while improving safety and performance and maintaining affordability. This program follows the UltraLight Steel Auto Body (ULSAB) program (results announced worldwide in 1998). As with the ULSAB Program, the ULSAB-AVC Consortium commissioned PORSCHE ENGINEERING SERVICES, INC., Troy, Mich. USA, to provide design and engineering management for ULSAB-AVC.

In the ULSAB-AVC program, PORSCHE ENGINEERING SERVICES, INC. takes a holistic approach to the development of a new vehicle architecture that offers cost-efficient steel solutions to mass reduction challenges. ULSAB-AVC will present advanced vehicle concepts to help automakers use steel more efficiently and provide a steel-based structural platform for achieving:

- Anticipated crash safety requirements for 2004,
- Significantly improved fuel efficiency,
- Optimized environmental performance regarding emissions, source reduction and recycling,
- High volume manufacturability at affordable cost.

Technical Transfer Dispatches (TTD)

To encourage valuable dialogue, the ULSAB-AVC Program provides periodic communications in the form of TTDs to key contacts within the automotive industry to keep key expert automotive staff informed about Program progress. TTD #6 provides critical information about the application of advanced high strength steels (AHSS) to vehicle design, offering important design considerations in using these advanced steels. Also included in this TTD are examples of the effective collaboration process between steel suppliers and design engineers to achieve the fully optimized use of AHSS and documentation of properties for the steel grades used in the ULSAB-AVC body structures.

It is important to note that the information reported in this dispatch related to ULSAB-AVC's design is work in progress, subject to change as the engineering process is completed. The final program results, to be delivered to the global automotive community in early 2002, could be different than what is included here. However, from our experience with previous dispatches, we believe that allowing our customers to review the work in progress not only provides an avenue for exchange and feedback but also contributes helpful input to our customers' own research efforts.

For more information or to provide feedback, please contact your local ULSAB-AVC Member Company or ULSAB-AVC program management as follows:

Ed Opbroek, Program Director
ULSAB-AVC
Tel. (513) 422-1844
Fax. (513) 424-0270
E-mail. EdOpbroek@ulsab.org

1.0 Introduction

Engineered steels provide automotive designers and manufacturers with the unique option of combining lightweighting with the traditional steel advantages of low cost and eco-efficiency. This was clearly demonstrated by the ULSAB Program and was achieved, in part, through the extensive use of both high strength steels (HSS) and ultra high strength steels (UHSS).

The HSS grades used in ULSAB utilized mostly conventional microalloy approaches. The goals for ULSAB-AVC are more aggressive than for ULSAB because of the need to reduce the added mass required to satisfy future safety mandates. For ULSAB-AVC, it is therefore appropriate to also consider the application of newer types of high strength steels, the so-called advanced high strength steels (AHSS), to assist in achieving the overall aims of the program through the design of an efficient lightweight body structure.

In contrast to ULSAB, where a key focus was to demonstrate the *manufacturing feasibility* of the aggressive use of readily available HSS and modern manufacturing processes (e.g. tailored blanks, hydroforming, assembly laser welding), ULSAB-AVC is a *concept* program. This provides an opportunity to expand the list of candidate steels by considering those steels that are currently available and those that will become available by 2004. To coordinate this, it was first necessary to adopt a consistent nomenclature of the various grades of steels.

1.1 ULSAB-AVC Steel Nomenclature

Methods used to classify steels vary considerably. To provide a consistent nomenclature, the ULSAB-AVC Consortium adopted a standard practice that defines both yield strength (YS) and ultimate tensile strength (UTS). In this classification system, steels are identified as:

XX aaa/bbb	Where	XX	= Type of steel
		aaa	= Minimum YS in MPa, and
		bbb	= Minimum UTS in MPa.

The steel type designator uses the following classification:

<u>Conventional Types</u>	<u>Advanced High Strength (AHSS) Types *</u>
Mild = Mild steel	DP = Dual phase
IF = Interstitial-free	CP = Complex phase
IS = Isotropic	TRIP = Transformation-induced plasticity
BH = Bake hardenable	Mart = Martensitic
CMn = Carbon-manganese	
HSLA = High strength, low alloy	* refer to Section 3.0 for further description

As an example, a classification of DP 500/800 refers to dual phase steel with 500 MPa minimum yield strength and 800 MPa minimum ultimate tensile strength.

1.2 The Rationale for Advanced High Strength Steels

Consistent with the terminology adopted for ULSAB, High Strength Steels (HSS) are defined as those steels with yield strengths from 210–550 MPa; Ultra-High Strength Steels (UHSS) are defined as steels with yield strengths greater than 550 MPa. The yield strengths of Advanced High Strength Steels (AHSS) overlap the range of strengths between HSS and UHSS, as shown in Figure 1. The principal differences between conventional HSS and AHSS are due to their microstructures. AHSS are multi-phase steels, which contain martensite, bainite, and/or retained austenite in quantities sufficient to produce unique mechanical properties. Compared to conventional micro-alloyed steels, AHSS exhibit a superior combination of high strength with good formability. This combination arises primarily from their high strain hardening capacity as a result of their lower yield strength (YS) to ultimate tensile strength (UTS) ratio.

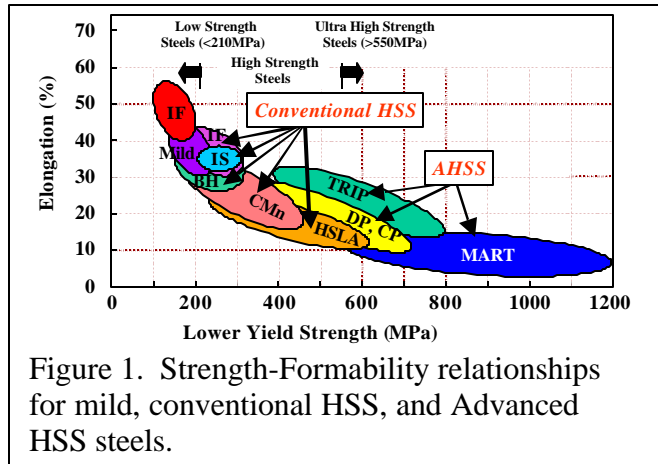


Figure 1. Strength-Formability relationships for mild, conventional HSS, and Advanced HSS steels.

For conventional steels, reduced formability is one of the consequences when selecting steels with higher strength levels. To overcome this, recent steel developments, which can facilitate further lightweighting of automotive structures, have targeted this phenomenon. The family of steels based on multi-phase microstructures typify the development of improved material concepts to enhance formability.

The multi-phase AHSS family includes dual phase (DP), transformation induced plasticity (TRIP) and complex phase (CP), products. Figure 1 data show the relative strengths and formability (measured by total elongation) of conventional strength steels, such as mild (Mild) and interstitial free (IF) steels; conventional HSS such as carbon-manganese (CMn), bake hardenable (BH), isotropic (IS), high strength IF (IF), high strength, low alloy (HSLA). Figure 1 also shows advanced high strength steels (AHSS) such as dual phase (DP), transformation induced plasticity (TRIP), complex phase (CP), and martensite (Mart) steels.

Although not displayed in Figure 1, another category of steels, known as press hardened or hot-formed steels are also of interest, especially for those components with a complicated shape but requiring ultra high strength levels. These grades are, essentially, martensitic grades.

2.0 Materials Selected for the ULSAB-AVC Body Structure

The materials selected for the ULSAB-AVC Body Structure are illustrated as Figure 2 (C-Class) and Figure 3 (PNGV-Class), with the steel grades selected collated as Table 1. The pie charts of Figure 4 enable a comparison to be made of the materials used in ULSAB and in ULSAB-AVC and indicate that the complete body structure of ULSAB-AVC is comprised of high strength steel. Stamping, roll forming and hydroforming are the only processes used for the manufacture of all components. Initially, it was considered that hot-formed steels would be required for some parts. However, component geometry (shape) modifications enabled all such parts to be replaced with components made by less expensive stamping or roll forming processes. A complete list of the materials selected for each part is provided as Appendix I, and the materials properties utilized provided as Appendix II.

The data of Figure 4 illustrate that the body structures of both the PNGV-Class and C-Class ULSAB-AVC designs utilize approximately 85% of Advanced High Strength Steels, with the clear majority of components being designed using dual phase steels. The relatively simple shapes of the components in this concept design had a significant influence on the types of steels selected. In particular, for a number of components, both DP and TRIP steels were viable candidates for selection. The choice of a less-costly DP grade was enabled since part geometry rendered the superior formability of TRIP steels redundant, based on the first-approximation one-step forming simulations. In the case of the floor pan, TRIP 450/800 was selected rather than a DP grade. This particular component undergoes significant deformation during manufacture, so that manufacturing feasibility will benefit from the additional forming capacity of the TRIP grade. In addition, practical experience on similar components has indicated that one step forming simulations may not be completely reliable in predicting the manufacturing feasibility for such components. The selection of TRIP 450/800, therefore, provides a greater margin of manufacturing feasibility than would be the case with DP grades.

It must, of course, be emphasized that ULSAB-AVC is only one possible solution to achieve lightweight steel body structures. Consequently, the particular AHSS selected for each component was based on the specific designs used in ULSAB-AVC. The steels selected should be considered as useful guidelines for similar components in other automotive designs. The material selected by other automotive manufacturers will be based on a balanced consideration of their specific factors — manufacturability, performance and cost. Based on ULSAB-AVC experience, component design is of paramount importance.

To provide for a deeper appreciation of the rationale for materials selection, the following sections provide an overview of the metallurgical concepts of AHSS and the selection process used in ULSAB-AVC, including the use of forming simulations to assess manufacturing feasibility.

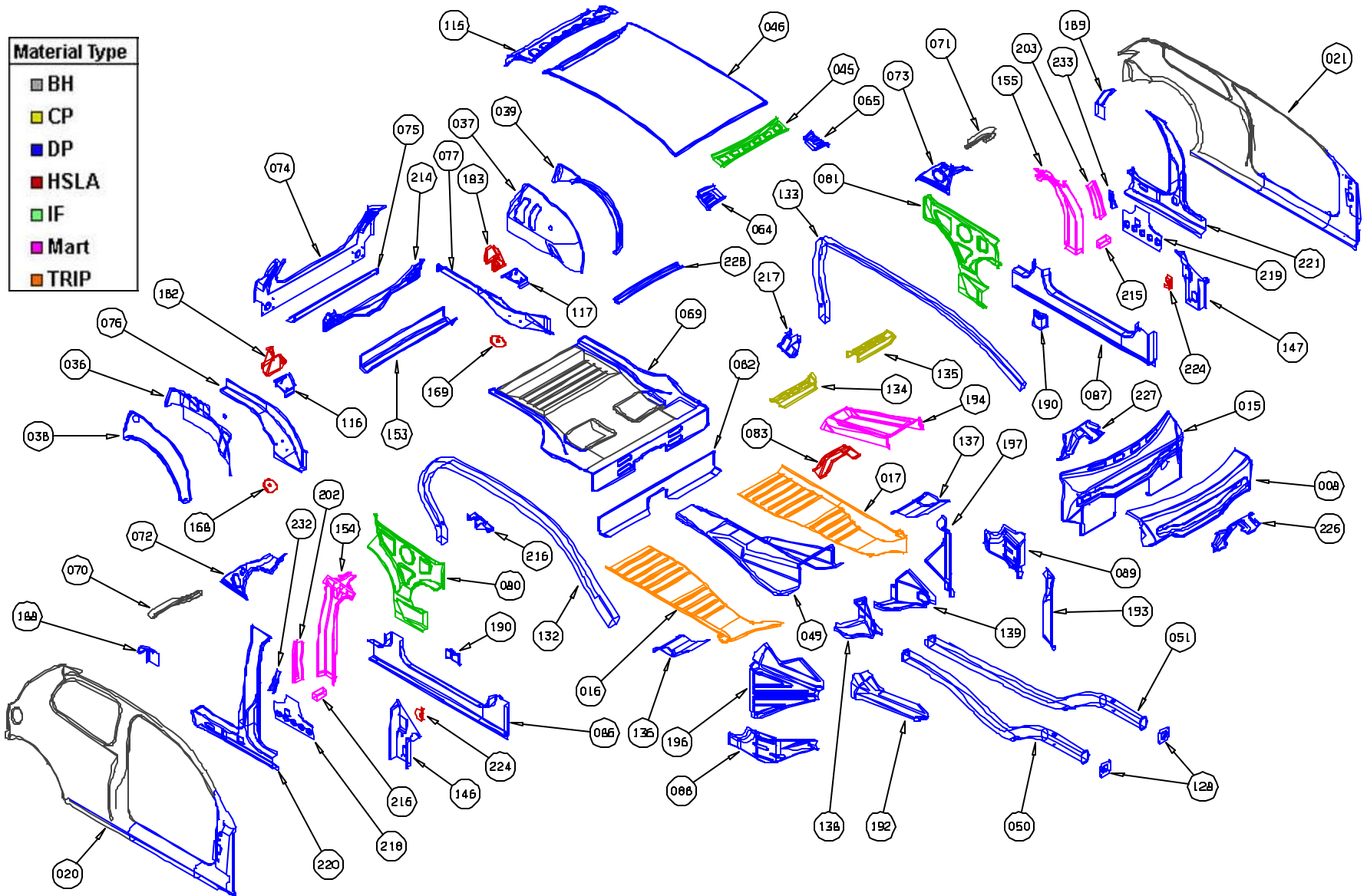


Figure 2. Exploded view of final ULSAB-AVC C-Class concept design, showing steel types selected for individual parts.

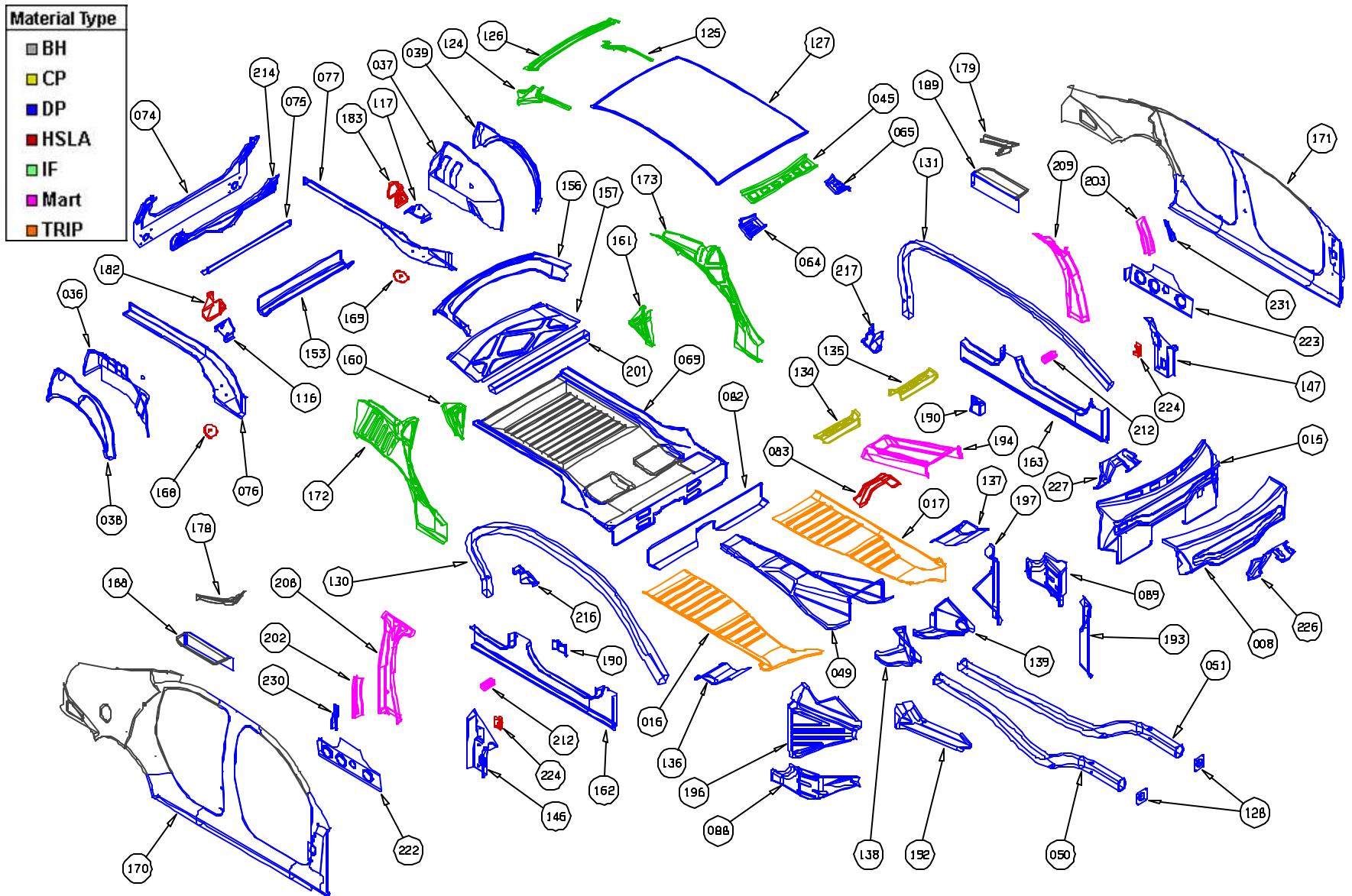


Figure 3. Exploded view of final ULSAB-AVC PNGV-Class concept design, showing steel types selected for individual parts.

Table 1. Steel Grades selected for the final ULSAB-AVC body structure concept design.

Steel Grade	YS (MPa)	UTS (MPa)	Total EL (%)	n-value ¹ (5-15%)	r-bar	K-value ² (MPa)
Flat sheet, as shipped properties						
BH 210/340	210	340	34-39	0.18	1.8	582
BH 260/370	260	370	29-34	0.13	1.6	550
DP 280/600	280	600	30-34	0.21	1.0	1082
IF 300/420	300	420	29-36	0.20	1.6	759
DP 300/500	300	500	30-34	0.16	1.0	762
HSLA 350/450	350	450	23-27	0.14	1.1	807
DP 350/600	350	600	24-30	0.14	1.0	976
DP 400/700	400	700	19-25	0.14	1.0	1028
TRIP 450/800	450	800	26-32	0.24	0.9	1690
DP 500/800	500	800	14-20	0.14	1.0	1303
CP 700/800	700	800	10-15	0.13	1.0	1380
DP 700/1000	700	1000	12-17	0.09	0.9	1521
Mart 950/1200	950	1200	5-7	0.07	0.9	1678
Mart 1250/1520	1250	1520	4-6	0.065	0.9	2021
Straight tubes, as shipped properties						
DP 280/600	450	600	27-30	0.15	1.0	1100
DP 500/800	600	800	16-22	0.10	1.0	1250
Mart 950/1200	1150	1200	5-7	0.02	0.9	1550

YS and UTS are minimum values, others are typical values

Total EL % - Flat Sheet (A50 or A80), Tubes (A5)

¹n-value is calculated in the range of 5 to 15% true strain.

²K-value is the magnitude of true stress extrapolated to a true strain of 1.0. It is a material property parameter frequently used by one-step forming simulation codes.

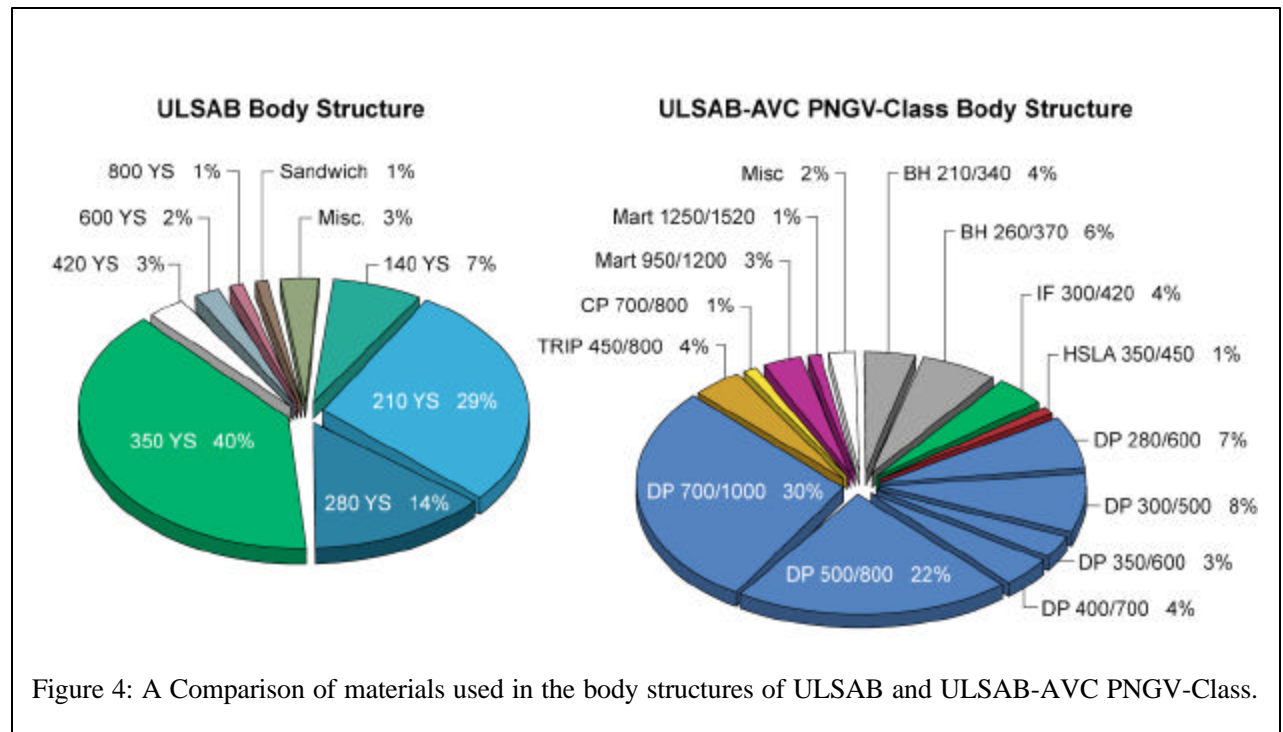


Figure 4: A Comparison of materials used in the body structures of ULSAB and ULSAB-AVC PNGV-Class.

3.0 AHSS Microstructure, Mechanical Behaviour, and Alloy Design

The fundamental metallurgy of conventional low- and high-strength steels is generally well understood by manufacturers and users of steel products. Since the metallurgy and processing of AHSS grades is, however, somewhat novel compared to conventional steels, they will be described briefly to provide a baseline understanding of how their unique mechanical properties evolve from their unique processing and structure.

3.1 Dual Phase (DP) Steels

The microstructure of dual phase (DP) steels is comprised of soft ferrite and, depending on strength, between 20 and 70% volume fraction of hard phases, normally martensite*. Figure 5 displays the microstructure of a DP ferrite + martensite steel with 350 MPa yield strength and 600 MPa. The soft ferrite phase is generally continuous, giving these steels excellent ductility. When these steels deform, however, strain is concentrated in the lower strength ferrite phase, creating the unique high work hardening rate exhibited by these steels.

The work hardening rate along with excellent elongation combine to give DP steels much higher ultimate tensile strength than conventional steels of similar yield strength. Figure 6 illustrates this, where the quasi-static stress-strain

behavior of high strength, low alloy (HSLA) steel is compared with that of a DP steel of similar yield strength. The DP steel exhibits higher initial work hardening rate, uniform and total elongation, ultimate tensile strength, and lower YS/TS ratio than the similar yield strength HSLA. DP and other AHSS also have another important benefit compared with conventional steels. The bake hardening effect, which is the increase in yield strength resulting from prestraining (representing the work hardening due to stamping or other manufacturing process) and elevated temperature aging (representing the curing temperature of paint bake ovens) continues to increase with increasing strain. Conventional bake hardening effects, of BH steels for example, remain somewhat constant after prestrains of about 2%. The extent of the bake hardening effect in AHSS depends on the specific chemistry and thermal histories of the steels. DP steels are designed to provide ultimate tensile strengths of up to 1000 MPa.

*In some instances, especially for hot rolled steels requiring enhanced capability to resist stretching on a blanked edge (as typically measured by hole expansion capacity), the microstructure can also contain significant quantities of bainite.

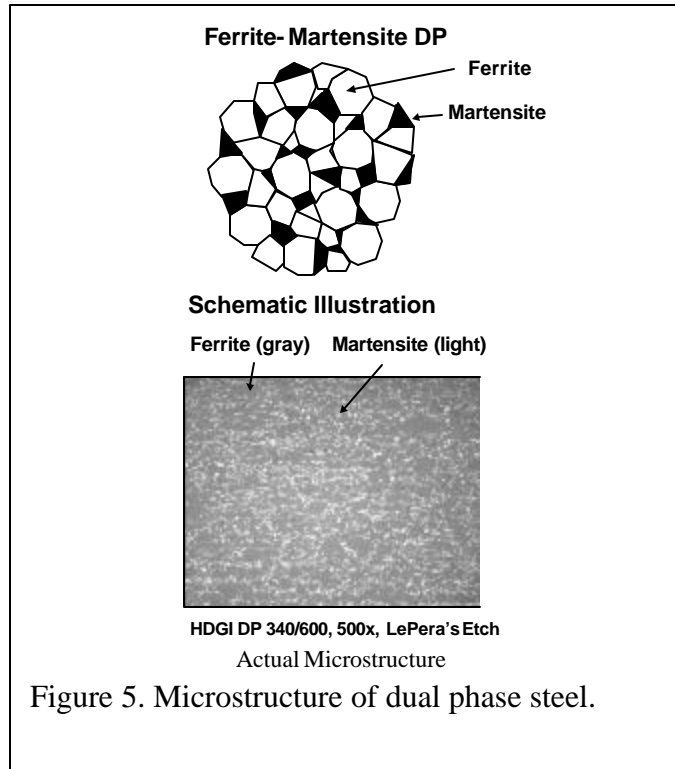


Figure 5. Microstructure of dual phase steel.

In DP steels, carbon enables the formation of martensite at practical cooling rates. That is, it increases the hardenability of the steel. Manganese, chromium, molybdenum, vanadium and nickel added individually or in combination also increase hardenability. Carbon also strengthens the martensite as a ferrite solute strengthener, as do silicon and phosphorus. Silicon also strengthens the martensite since it helps to partition carbon to the austenite to increase its hardenability and the strength of the resultant martensite phase. These additions are carefully balanced, not only to produce unique mechanical properties, but also to minimize any difficulties with resistance spot welding, which is, in general good. However, when welding the highest strength grade (DP 700/1000) to itself, the spot weldability may require welding practice adjustments.

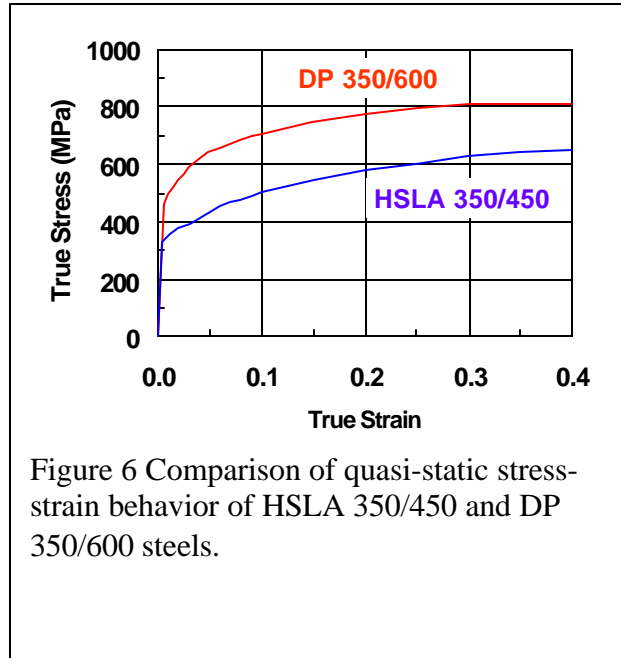


Figure 6 Comparison of quasi-static stress-strain behavior of HSLA 350/450 and DP 350/600 steels.

3.2 Transformation Induced Plasticity (TRIP) Steels

The microstructure of TRIP steels consists of a continuous ferrite matrix containing a dispersion of hard second phases--martensite and/or bainite. These steels also contain retained austenite in volume fractions greater than 5%. A typical TRIP steel microstructure is shown in Figure 7.

During deformation, the dispersion of hard second phases in soft ferrite creates a high work hardening rate, as observed in the DP steels. However, in TRIP steels, the retained austenite also progressively transforms to martensite with increasing strain, thereby increasing the work hardening rate at higher strain levels. This is schematically illustrated in Figure 8, where the stress-strain behavior of HSLA, DP and TRIP steels of approximately similar yield strengths are compared. The TRIP steel has a lower initial work hardening rate than the DP steel, but the hardening rate persists at higher strains where that of the DP begins to diminish.

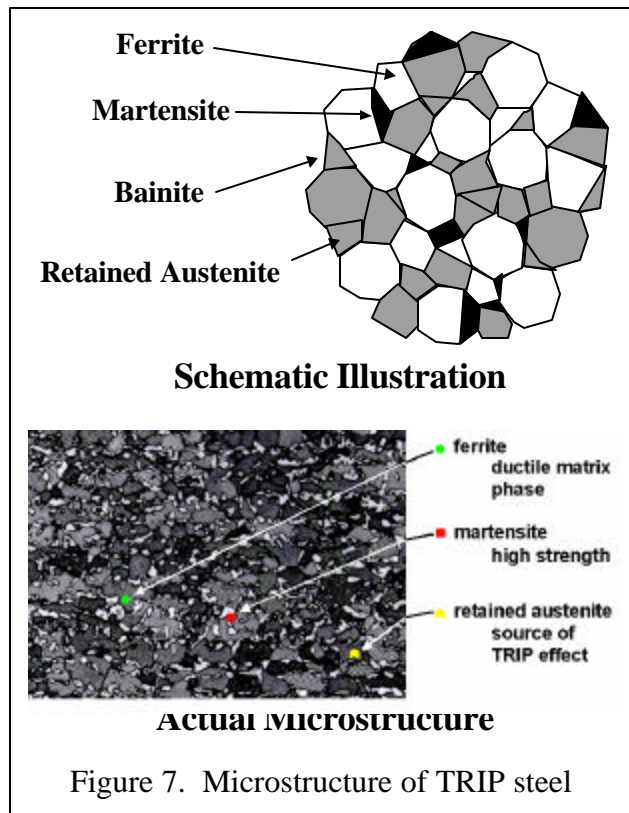


Figure 7. Microstructure of TRIP steel

The work hardening rates of DP and TRIP steels are substantially higher than for conventional HSS, providing DP and TRIP with significant formability advantages. This is particularly useful when designers take advantage of the high work hardening rate (and increased Bake Hardening effect) and design to as-formed mechanical properties. High work hardening rate persists to higher strains in TRIP steels, providing a slight advantage over DP in the most severe stretch forming applications.

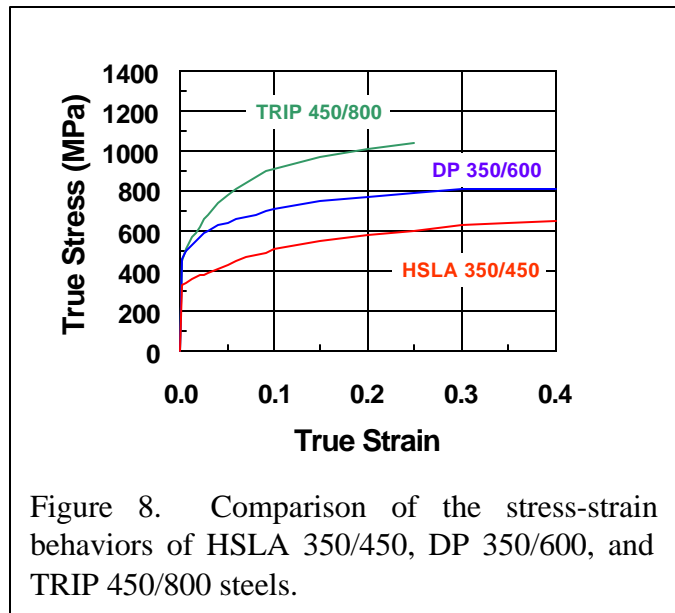


Figure 8. Comparison of the stress-strain behaviors of HSLA 350/450, DP 350/600, and TRIP 450/800 steels.

TRIP steels use higher quantities of carbon and silicon and/or aluminum than DP steels to lower the martensite finish

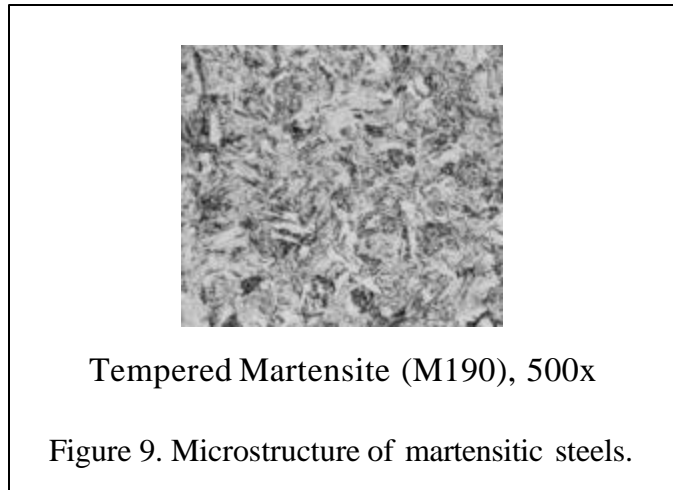
temperature to below ambient temperatures to form the retained austenite phase. The strain level at which retained austenite begins to transform to martensite can be designed by adjusting carbon content. At lower carbon levels, the retained austenite begins to transform almost immediately upon deformation, increasing work hardening rate and formability during the stamping process. At higher carbon contents, the retained austenite is more stable and begins to transform only at strain levels beyond those produced during stamping and forming. At these carbon levels the retained austenite persists into the final part. It transforms to martensite during subsequent deformation, such as a crash event, and provides greater crash energy absorption. TRIP steels can therefore be engineered or tailored to provide excellent formability for manufacturing complex AHSS parts or to exhibit high work hardening during crash deformation to provide excellent crash energy absorption. The additional alloying requirements of TRIP steels degrade their resistance spot welding behavior. This can be addressed somewhat by modification of the welding cycles used (for example, pulsating welding or dilution welding).

3.3 Complex Phase (CP) Steels

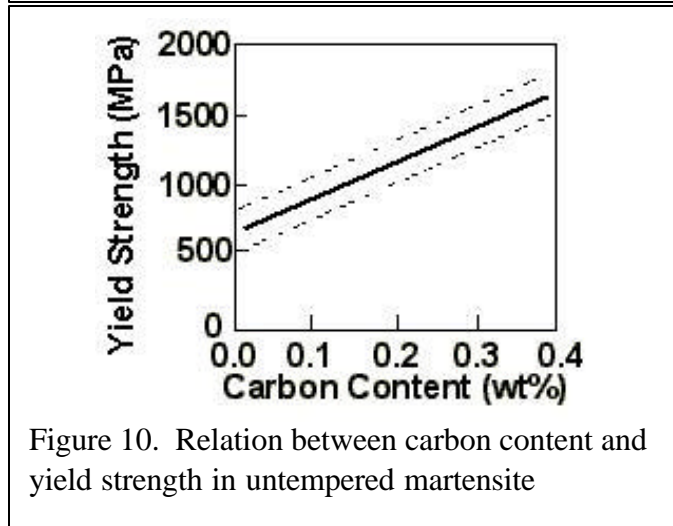
Complex phase steels typify the transition to steel with very high ultimate tensile strengths. CP steels consist of a very fine microstructure of ferrite and a higher volume fraction of hard phases, that are further strengthened by fine precipitates. They use many of the same alloy elements found in DP and TRIP steels, but additionally have small quantities of niobium, titanium and/or vanadium to form fine strengthening precipitates. Complex phase steels provide ultimate tensile strengths of 800 MPa and greater. Under the conditions of strain and strain rates typically encountered in a crash, this AHSS absorbs greater energy. Complex phase steels are characterized by high deformability, high energy absorption, and high residual deformation capacity. Typical candidate applications for CP steels are those that require high energy absorption capacity in the elastic and low-plastic range, such as bumper and B-Pillar reinforcements.

3.4 Martensitic (Mart) Steels

In martensitic steels, the austenite that exists during hot rolling or annealing is transformed almost entirely to martensite during quenching on the run-out table or in the cooling section of the annealing line. (This structure can also be developed with post-forming heat treatment) Martensitic steel microstructure largely contains lath martensite as shown in Figure 9.



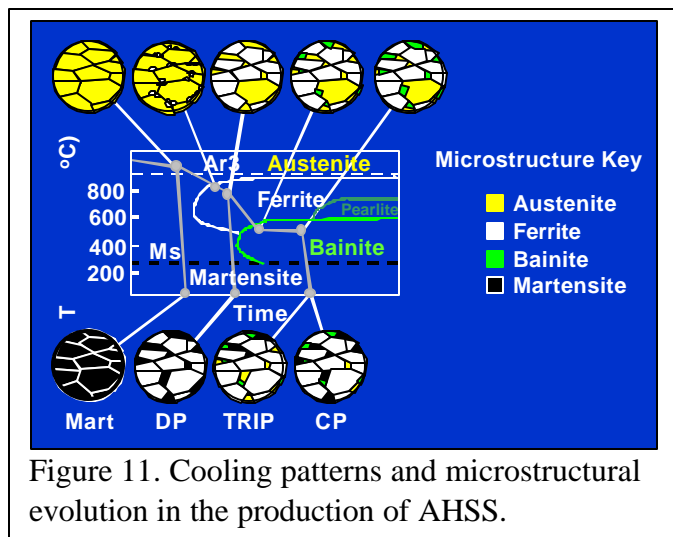
Martensitic steels provide the highest strengths, up to 1500 MPa ultimate tensile strengths. Martensitic steels are often subjected to post-quench tempering to improve ductility, and can provide remarkable formability even at extremely high strengths.



Carbon is added to martensitic steels to increase hardenability and also to strengthening the martensite. The data of Figure 10 (5) illustrate the relationship between carbon content and 0.2% offset yield strength in untempered martensite. Manganese, silicon, chromium, molybdenum, boron, vanadium, and nickel are also used in various combinations to increase hardenability.

3.5 Advanced High Strength Steel Processing

All AHSS are produced by controlling the cooling rate from the austenite or austenite plus ferrite phase, either on the runout table of the hot mill (for hot rolled products) or in the cooling section of the continuous annealing furnace (continuously annealed or hot dip coated products). AHSS cooling patterns and resultant microstructures are schematically illustrated on the continuous cooling-transformation diagram. See in Figure 11. Martensitic steels are produced from the austenite phase by rapid quenching to



transform most of the austenite to martensite. Dual phase ferrite + martensite steels are produced by controlled cooling from the austenite phase (in hot rolled products) or from the two-phase ferrite + austenite phase (for continuously annealed and hot dip coated products) to transform some austenite to ferrite before rapid cooling to transform the remaining austenite to martensite. TRIP steels typically require the use of an isothermal hold at an intermediate temperature, which produces some bainite. The higher silicon and carbon content of TRIP steels also results in significant volume fractions of retained austenite in the final microstructure. Complex phase steels also follow a similar cooling pattern, but here, the chemistry is adjusted to produce less retained austenite and form fine precipitates to strengthen the martensite and bainite phases.

4.0 Materials Selection Process for ULSAB-AVC

The materials selection process used in ULSAB-AVC was significantly different from that employed in ULSAB. For the ULSAB Program, the design was based on static mechanical properties and utilized commonly available materials, since it was in large measure a validation-of-concepts exercise.

It is well known that steels display positive strain rate dependence. That is, at the higher rates of strain typically associated with, for example, crash events, steels have higher strengths and consequently higher energy absorption. Preliminary studies (see also Appendix III) confirmed that utilization of this phenomenon could assist in lightweighting. Accordingly, it was decided to utilize this experience in the design of the body structure of ULSAB-AVC. In addition, because of the relative new use of AHSS for automotive applications, it was also determined that the engineering experience of the vehicle designers would be supplemented with analytical FEA simulations to assess forming behavior.

Steel members of the ULSAB-AVC Consortium were initially surveyed as to steels currently available, those under development and those anticipated to be available by 2004. These materials were compiled along with their associated high strain rate properties and utilized in the initial C-Class and PNGV-Class body structure concept designs. These initial designs were based on yield strength considerations. In the final concept design, specific grades of AHSS were selected in a manner that best paired their unique mechanical properties with the structural demands of specific ULSAB-AVC components. A detailed description of the considerations used to select AHSS for ULSAB-AVC applications is described in Appendix III.

5.0 Forming Assessment

To assess the forming behavior of the steels selected, one step forming simulations were performed for all major components. The key focus of these analyses was to provide simultaneous engineering assistance to Porsche Engineering Services, Inc. (PES) to:

- Assess formability of the part and evaluate possible changes in design
- Facilitate the selection of steels for applications traditionally considered very difficult or impossible to form, based on engineering experience
- Identify alternative steel grades to facilitate down-gauging
- Identify alternatives to expensive materials or processes, such as press-hardened grades.

One-step forming simulation provides a first approximation of forming behavior but does not take into account tooling geometry and boundary conditions. The one-step analyses indicated that the initial concept designs were feasible and provided PES with confidence in the appropriateness of their concept designs; the one-step analyses also identified opportunities for further reductions in mass (through down gauging) and materials costs. The concept design then underwent a series of evolutions to optimize safety or crash performance, stiffness and mass. In some instances, these evolutions resulted in significant modifications of some components and required, for example, the use of tailor welded blanks. To validate the manufacturing feasibility of these changes, selected components were also subjected to forming simulation. Illustrative examples of these forming simulations are collated as Appendix IV.

**ULSAB-AVC
Advanced Vehicle Concepts**

Technical transfer Dispatch #6 (TTD6)

Appendix I - ULSAB-AVC Body Structure Parts List

ULSAB-AVC Body Structure Parts List

Revision Level: A20 Date: 26APR01 TTD6

Part Number			Name	Blank No.	Gage (mm)	Material Type	Grade (MPa)		Manuf. Process Code	Designed Mass (kg)	
							Yield Strength	Tensile Strength		C-Class	D/E-Class
AVC	1	1008	Cowl Front		0.80	DP	500	800	S	4.416	4.416
AVC	1	1015	Dash		0.65	DP	280	600	S	4.381	4.381
AVC	1	1045	Header Front		0.70	IF	300	420	S	0.686	0.686
AVC	1	1064	Support Header Front RH		0.70	DP	280	600	S	0.231	0.231
AVC	1	1065	Support Header Front LH		0.70	DP	280	600	S	0.231	0.231
AVC	1	1075	Crossmember Back Panel		0.65	DP	280	600	S	0.832	0.832
AVC	1	1082	Crossmember Kick-Up		0.70	DP	700	1000	S	2.002	2.002
AVC	1	1083	Crossmember Tunnel		0.70	HSLA	350	450	S	0.602	0.602
AVC	1	1088	Bulkhead Crash Box Dash RH		1.20	DP	700	1000	S	2.376	2.376
AVC	1	1089	Bulkhead Crash Box Dash LH		1.20	DP	700	1000	S	2.376	2.376
AVC	1	1116	Assy Reinf Rail Rear Suspension Attach RH		1.30	DP	500	800	S	0.455	0.455
AVC	1	1117	Assy Reinf Rail Rear Suspension Attach LH		1.30	DP	500	800	S	0.455	0.455
AVC	1	1128	Plate Crash Box Rail Front Attach (x2)		3.00	DP	700	1000	S	0.600	0.600
AVC	1	1134	Crossmember Support Front Seat Front RH		0.70	CP	700	800	S	0.567	0.567
AVC	1	1135	Crossmember Support Front Seat Front LH		0.70	CP	700	800	S	0.567	0.567
AVC	1	1136	Closeout Lower Crash Box Dash RH		0.90	DP	500	800	S	1.161	1.161
AVC	1	1137	Closeout Lower Crash Box Dash LH		0.90	DP	500	800	S	1.161	1.161
AVC	1	1138	Closeout Inner Crash Box Dash RH		0.80	DP	400	700	S	1.072	1.072
AVC	1	1139	Closeout Inner Crash Box Dash LH		0.80	DP	400	700	S	1.040	1.040
AVC	1	1146	A-Post Inner RH		0.90	DP	700	1000	S	1.152	1.152
AVC	1	1147	A-Post Inner LH		0.90	DP	700	1000	S	1.152	1.152
AVC	1	1153	Crossmember Rear Suspension		1.00	DP	700	1000	S	2.640	2.640
AVC	1	1168	Reinf Rail Rear Spring Attach RH		1.20	HSLA	350	450	S	0.144	0.144
AVC	1	1169	Reinf Rail Rear Spring Attach LH		1.20	HSLA	350	450	S	0.144	0.144
AVC	1	1182	Reinf Rail Rear Suspension C-Member RH		1.50	HSLA	350	450	S	0.765	0.765
AVC	1	1183	Reinf Rail Rear Suspension C-Member LH		1.50	HSLA	350	450	S	0.765	0.765
AVC	1	1190	Bracket Support Front Seat Rear (x2)		1.20	DP	500	800	S	0.576	0.576
AVC	1	1192	Reinf Crash Box Dash RH		1.00	DP	400	700	S	1.170	1.170
AVC	1	1193	Reinf Crash Box Dash LH		1.00	DP	400	700	S	1.170	1.170
AVC	1	1194	Reinf Tunnel		0.70	Mart	950	1200	S	2.394	2.394
AVC	1	1196	Closeout Outer Crash Box Dash RH		0.80	DP	400	700	S	2.344	2.344
AVC	1	1197	Closeout Outer Crash Box Dash LH		0.80	DP	400	700	S	2.344	2.344
AVC	1	1202	Reinf Waist B-Pillar Inner RH		1.50	Mart	1250	1520	S	0.885	0.885
AVC	1	1203	Reinf Waist B-Pillar Inner LH		1.50	Mart	1250	1520	S	0.885	0.885
AVC	1	1216	Bracket Member Body Side Inner Att Rear RH		1.20	DP	500	800	S	0.396	0.396
AVC	1	1217	Bracket Member Body Side Inner Att Rear LH		1.20	DP	500	800	S	0.396	0.396
AVC	1	1224	Bracket Crossmember Inst Panel Attach RH		1.20	HSLA	350	450	S	0.132	0.132
AVC	1	1225	Bracket Crossmember Inst Panel Attach LH		1.20	HSLA	350	450	S	0.132	0.132
AVC	1	1226	A-Brace Cowl Front		1.00	DP	500	800	S	0.980	0.980
AVC	1	1227	A-Brace Cowl Rear		1.00	DP	500	800	S	0.820	0.820
AVC	2	1016	Floor Front RH		0.65	TRIP	450	800	S	4.219	
AVC	2	1017	Floor Front LH		0.65	TRIP	450	800	S	4.219	
AVC	2	1020	Body Side Outer RH	1	1.50	DP	700	1000	S/TWB	3.645	
				2	0.70	BH	260	370		8.358	
				3	1.80	DP	700	1000		3.618	
AVC	2	1021	Body Side Outer LH	1	1.50	DP	700	1000	S/TWB	3.645	
				2	0.70	BH	260	370		8.414	
				3	1.80	DP	700	1000		3.618	
AVC	2	1036	Wheelhouse Inner RH	1	0.60	DP	500	800	S/TWB	1.320	
				2	1.40	DP	700	1000		0.966	
				3	1.10	DP	700	1000		0.616	
AVC	2	1037	Wheelhouse Inner LH	1	0.60	DP	500	800	S/TWB	1.320	
				2	1.40	DP	700	1000		0.966	
				3	1.10	DP	700	1000		0.616	
AVC	2	1038	Wheelhouse Outer RH		0.60	DP	280	600	S	1.074	
AVC	2	1039	Wheelhouse Outer LH		0.60	DP	280	600	S	1.092	
AVC	2	1046	Roof		0.65	DP	300	500	HFS	9.464	
AVC	2	1049	Tunnel		0.65	DP	300	500	S	5.122	
AVC	2	1050	Member Rail Front RH	1	1.50	DP Tube	500	800	HFT/TWT	1.845	
				2	1.30	DP Tube	500	800		6.331	
AVC	2	1051	Member Rail Front LH	1	1.50	DP Tube	500	800	HFT/TWT	1.845	
				2	1.30	DP Tube	500	800		6.331	
AVC	2	1069	Floor Rear	1	0.60	BH	210	340	S/TWB	5.838	
				2	1.10	DP	350	600		2.519	
				3	1.10	DP	350	600		2.255	
				4	0.70	DP	700	1000		1.988	

ULSAB-AVC Body Structure Parts List

Revision Level: A20 Date: 26APR01 TTD6

Part Number		Name	Blank No.	Gage (mm)	Material Type	Grade (MPa)		Manuf. Process Code	Designed Mass (kg)		
						Yield Strength	Tensile Strength		C-Class	D/E-Class	
AVC	2	1070	Gutter C-Pillar RH		0.65	BH	210	340	S	0.403	
AVC	2	1071	Gutter C-Pillar LH		0.65	BH	210	340	S	0.403	
AVC	2	1072	C-Pillar Inner RH		0.65	DP	500	800	S	0.774	
AVC	2	1073	C-Pillar Inner LH		0.65	DP	500	800	S	0.774	
AVC	2	1074	Back Panel		0.60	DP	300	500	S	2.532	
AVC	2	1076	Rail Rear RH	1	1.80	DP	700	1000	S/TWB	3.168	
				2	1.10	DP	500	800		0.737	
AVC	2	1077	Rail Rear LH	1	1.80	DP	700	1000	S/TWB	3.168	
				2	1.10	DP	500	800		0.737	
AVC	2	1080	Body Side Inner Rear RH		0.70	IF	300	420	S	2.541	
AVC	2	1081	Body Side Inner Rear LH		0.70	IF	300	420	S	2.541	
AVC	2	1086	Rocker Inner RH	1	1.50	DP	700	1000	S/TWB	1.815	
				2	0.70	DP	700	1000		2.345	
AVC	2	1087	Rocker Inner LH	1	1.50	DP	700	1000	S/TWB	1.815	
				2	0.70	DP	700	1000		2.345	
AVC	2	1115	Header Rear		0.65	DP	350	600	S	1.807	
AVC	2	1132	Member Body Side Inner RH		1.00	DP Tube	500	800	HFT	7.120	
AVC	2	1133	Member Body Side Inner LH		1.00	DP Tube	500	800	HFT	7.120	
AVC	2	1154	B-Pillar Inner RH		0.70	Mart	950	1200	S	1.610	
AVC	2	1155	B-Pillar Inner LH		0.70	Mart	950	1200	S	1.610	
AVC	2	1188	Rail Rear Outer Floor Extension RH		1.10	DP	500	800	S	0.319	
AVC	2	1189	Rail Rear Outer Floor Extension LH		1.10	DP	500	800	S	0.319	
AVC	2	1214	Support Back Panel		0.60	DP	300	500	S	1.020	
AVC	2	1215	Extension C-Member Kick-Up (x2)		1.20	Mart Tube	950	1200	ST	0.480	
AVC	2	1218	Reinf B-Pillar Lower RH		0.70	DP	700	1000	S	0.595	
AVC	2	1219	Reinf B-Pillar Lower LH		0.70	DP	700	1000	S	0.595	
AVC	2	1220	Reinf B-Pillar Rocker Rear RH	1	1.20	DP	700	1000	S/TWB	3.216	
				2	1.40	DP	700	1000		2.184	
AVC	2	1221	Reinf B-Pillar Rocker Rear LH	1	1.20	DP	700	1000	S/TWB	3.216	
				2	1.40	DP	700	1000		2.184	
AVC	2	1228	Crossmember Roof		0.70	DP	700	1000	S	0.490	
AVC	2	1232	Reinf Waist B-Pillar Outer RH		0.80	DP	700	1000	S	0.104	
AVC	2	1233	Reinf Waist B-Pillar Outer LH		0.80	DP	700	1000	S	0.104	
AVC	3	1016	Floor Front RH		0.65	TRIP	450	800	S		4.459
AVC	3	1017	Floor Front LH		0.65	TRIP	450	800	S		4.459
AVC	3	1036	Wheelhouse Inner RH	1	0.60	DP	500	800	S/TWB	1.356	
				2	1.40	DP	700	1000		0.966	
				3	1.10	DP	700	1000		0.660	
AVC	3	1037	Wheelhouse Inner LH	1	0.60	DP	500	800	S/TWB	1.356	
				2	1.40	DP	700	1000		0.966	
				3	1.10	DP	700	1000		0.660	
AVC	3	1038	Wheelhouse Outer RH		0.60	DP	280	600	S	1.134	
AVC	3	1039	Wheelhouse Outer LH		0.60	DP	280	600	S	1.146	
AVC	3	1049	Tunnel		0.65	DP	300	500	S	5.252	
AVC	3	1050	Member Rail Front RH	1	1.50	DP Tube	500	800	HFT/TWT	1.845	
				2	1.30	DP Tube	500	800		6.604	
AVC	3	1051	Member Rail Front LH	1	1.50	DP Tube	500	800	HFT/TWT	1.845	
				2	1.30	DP Tube	500	800		6.604	
AVC	3	1069	Floor Rear	1	0.60	BH	210	340	S/TWB	7.932	
				2	1.10	DP	350	600		3.135	
				3	1.10	DP	350	600		2.882	
				4	0.70	DP	700	1000		2.002	
AVC	3	1074	Back Panel		0.60	DP	300	500	S	2.172	
AVC	3	1076	Rail Rear RH	1	1.80	DP	700	1000	S/TWB	3.168	
				2	1.10	DP	500	800		1.408	
AVC	3	1077	Rail Rear LH	1	1.80	DP	700	1000	S/TWB	3.168	
				2	1.10	DP	500	800		1.408	
AVC	3	1124	Support Header Rear RH		0.70	IF	300	420	S	0.336	
AVC	3	1125	Support Header Rear LH		0.70	IF	300	420	S	0.336	
AVC	3	1126	Header Rear		0.70	IF	300	420	S	0.938	
AVC	3	1127	Roof		0.65	DP	300	500	HFS	8.905	
AVC	3	1130	Member Body Side Inner RH		1.00	DP Tube	500	800	HFT	7.070	
AVC	3	1131	Member Body Side Inner LH		1.00	DP Tube	500	800	HFT	7.070	
AVC	3	1156	Package Tray Upper		0.60	DP	280	600	S	2.316	
AVC	3	1157	Package Tray Lower		0.60	DP	280	600	S	2.208	

ULSAB-AVC Body Structure Parts List

Revision Level: A20 Date: 26APR01 TTD6

Part Number	Name	Blank No.	Gage (mm)	Material Type	Grade (MPa)		Manuf. Process Code	Designed Mass (kg)	
					Yield Strength	Tensile Strength		C-Class	D/E-Class
AVC 3 1160	Support Package Tray Lower RH		1.20	IF	300	420	S		0.852
AVC 3 1161	Support Package Tray Lower LH		1.20	IF	300	420	S		0.852
AVC 3 1162	Rocker Inner RH	1	1.50	DP	700	1000	S/TWB		1.815
		2	0.70	DP	700	1000			2.527
AVC 3 1163	Rocker Inner LH	1	1.50	DP	700	1000	S/TWB		1.815
		2	0.70	DP	700	1000			2.527
AVC 3 1170	Body Side Outer RH	1	1.50	DP	700	1000	S/TWB		3.645
		2	0.70	BH	260	370			0.280
		3	1.80	DP	700	1000			9.108
		4	1.20	DP	700	1000			2.148
		5	0.70	BH	260	370			5.649
AVC 3 1171	Body Side Outer LH	1	1.50	DP	700	1000	S/TWB		3.645
		2	0.70	BH	260	370			0.280
		3	1.80	DP	700	1000			9.108
		4	1.20	DP	700	1000			2.148
		5	0.70	BH	260	370			5.712
AVC 3 1172	Body Side Inner Rear RH		0.70	IF	300	420	S		2.555
AVC 3 1173	Body Side Inner Rear LH		0.70	IF	300	420	S		2.555
AVC 3 1178	Gutter Deck Lid RH		0.70	BH	260	370	S		0.385
AVC 3 1179	Gutter Deck Lid LH		0.70	BH	260	370	S		0.385
AVC 3 1188	Rail Rear Outer Floor Extension RH	1	1.10	DP	500	800	S/TWB		0.913
		2	0.60	BH	210	340			0.378
AVC 3 1189	Rail Rear Outer Floor Extension LH	1	1.10	DP	500	800	S/TWB		0.913
		2	0.60	BH	210	340			0.378
AVC 3 1201	Crossmember Package Tray		1.00	DP Tube	280	600	ST		2.540
AVC 3 1208	B-Pillar Inner RH		0.70	Mart	950	1200	S		1.491
AVC 3 1209	B-Pillar Inner LH		0.70	Mart	950	1200	S		1.491
AVC 3 1212	Extension C-Member Supt Front Seat Rr (x2)		1.20	Mart Tube	950	1200	ST		0.456
AVC 3 1214	Support Back Panel		0.60	DP	300	500	S		1.068
AVC 3 1222	Reinf B-Pillar Lower RH		1.00	DP	700	1000	S		1.430
AVC 3 1223	Reinf B-Pillar Lower LH		1.00	DP	700	1000	S		1.430
AVC 3 1230	Reinf Waist B-Pillar Outer RH		0.80	DP	700	1000	S		0.120
AVC 3 1231	Reinf Waist B-Pillar Outer LH		0.80	DP	700	1000	S		0.120
AVC - 1900	Brackets, Reinforcements and Hinges Estimated (not designed)							3.746	5.042
TOTAL								201.776	218.124

Code	Manufacturing Process
S	Stamped
S/TWB	Stamped / Tailor Welded Blanks
HFT	Hydroformed Tube
HFT/TWT	Hydroformed Tube / Tailor Welded Tubes
HFS	Hydroformed Sheet
RF	Roll Formed
ST	Straight or Shaped Tube

Code	Steel Types
BH	Bake Hardenable
CMn	Carbon Manganese
CP	Complex Phase
DP	Dual Phase
HSLA	High Strength, Low Alloy
IF	Interstitial-Free
IS	Isotropic Steel
Mart	Martensitic
Mild	Mild Steel
PrHd	Press Hardening
TRIP	Transformation-Induced Plasticity

**ULSAB-AVC
Advanced Vehicle Concepts**

Technical transfer Dispatch #6 (TTD6)

Appendix II - ULSAB-AVC Steel Grades Portfolio

ULSAB-AVC Steel Grades Portfolio

Steel Grade	YS (MPa)	UTS (MPa)	Total EL (%)	n-value ¹ (5-15%)	r-bar	K-value ² (MPa)
	(flat sheet, as shipped properties)					
BH 210/340	210	340	34-39	0.18	1.8	582
BH 260/370	260	370	29-34	0.13	1.6	550
DP 280/600	280	600	30-34	0.21	1.0	1082
IF 300/420	300	420	29-36	0.20	1.6	759
DP 300/500	300	500	30-34	0.16	1.0	762
HSLA 350/450	350	450	23-27	0.14	1.1	807
DP 350/600	350	600	24-30	0.14	1.0	976
DP 400/700	400	700	19-25	0.14	1.0	1028
TRIP 450/800	450	800	26-32	0.24	0.9	1690
DP 500/800	500	800	14-20	0.14	1.0	1303
CP 700/800	700	800	10-15	0.13	1.0	1380
DP 700/1000	700	1000	12-17	0.09	0.9	1521
Mart 950/1200	950	1200	5-7	0.07	0.9	1678
Mart 1250/1520	1250	1520	4-6	0.065	0.9	2021
	(straight tubes, as shipped properties)					
DP 280/600	450	600	27-30	0.15	1.0	1100
DP 500/800	600	800	16-22	0.10	1.0	1250
Mart 950/1200	1150	1200	5-7	0.02	0.9	1550

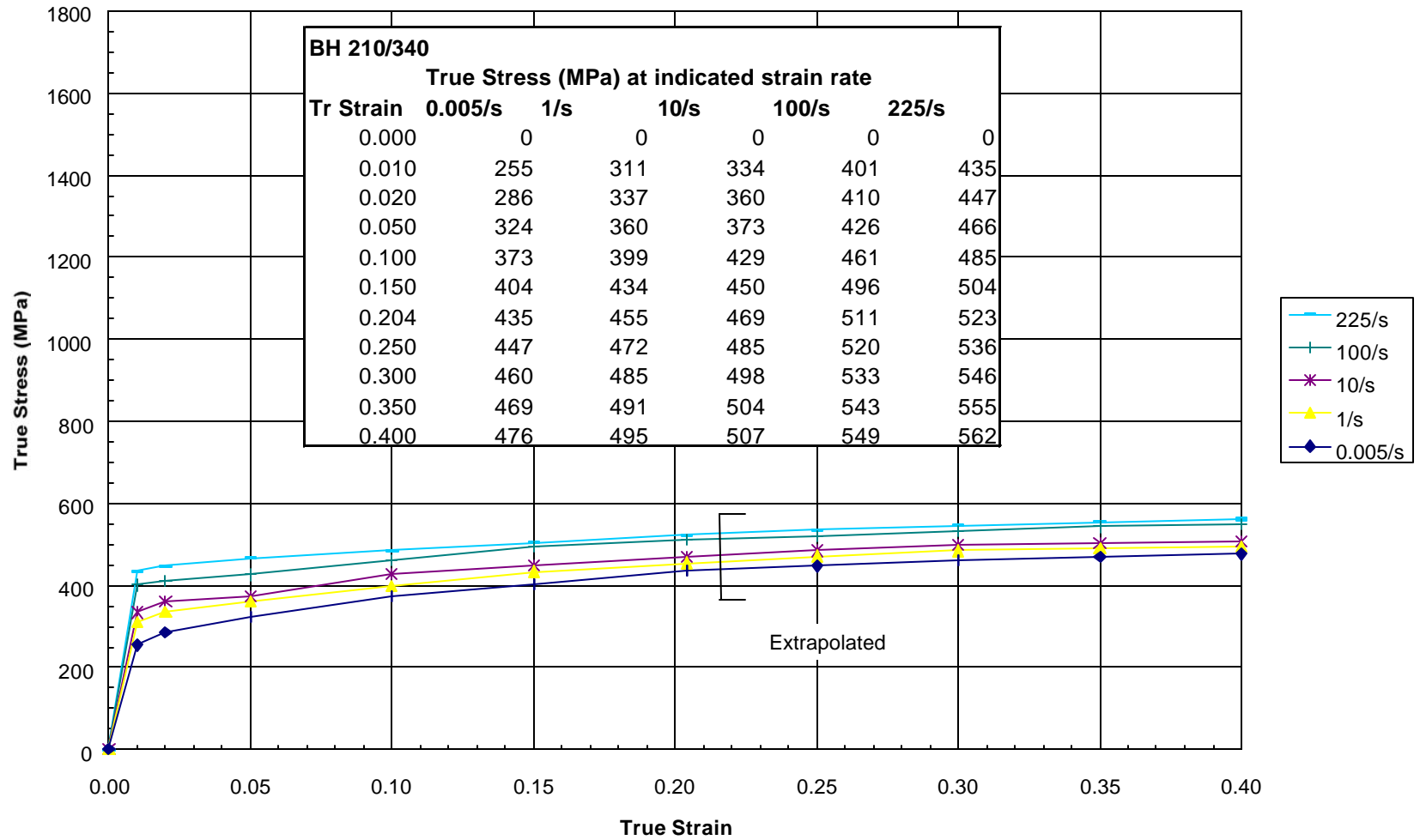
YS and UTS are minimum values, others are typical values

Total EL % - Flat Sheet (A50 or A80), Tubes (A5)

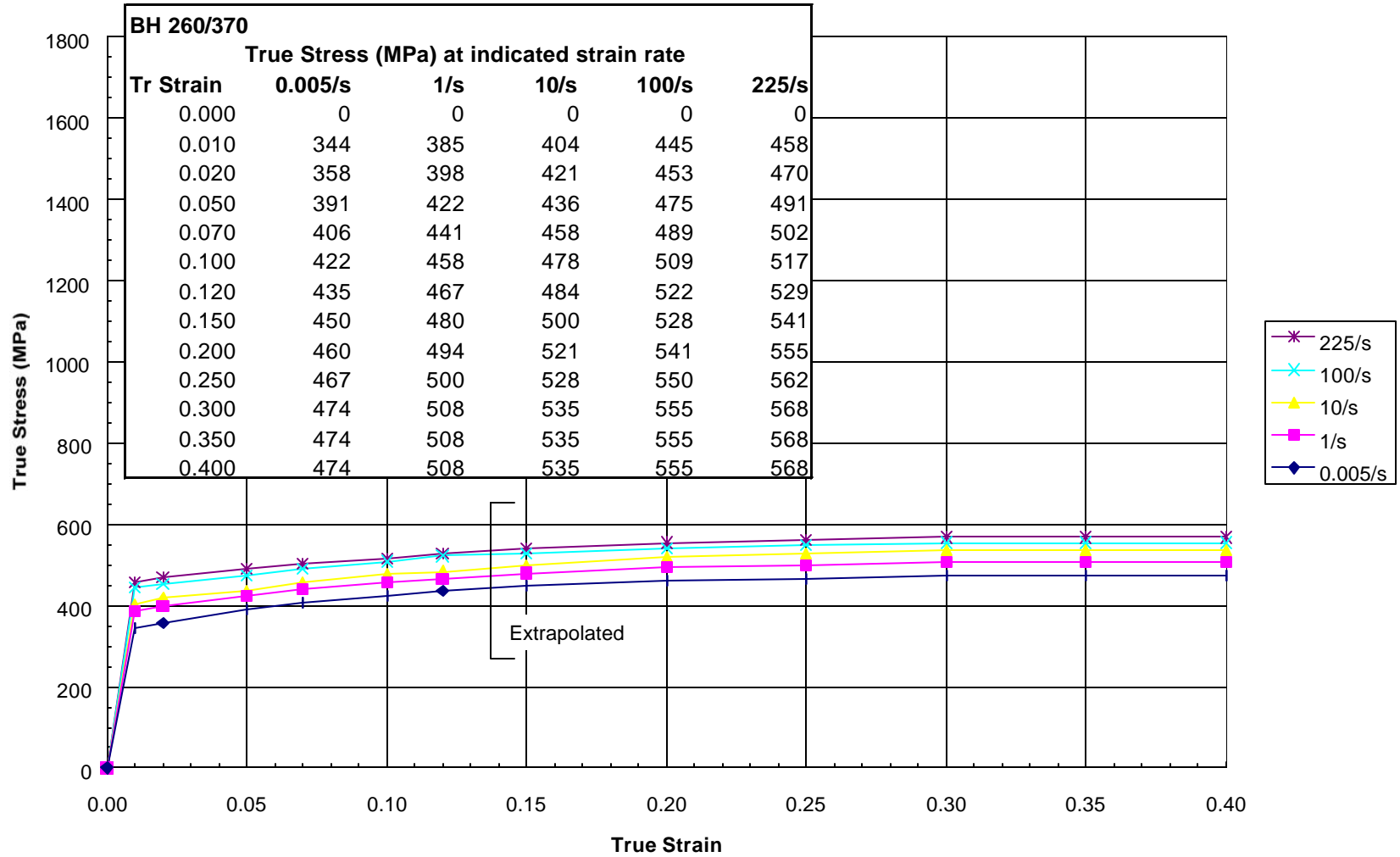
¹n-value is calculated in the range of 5 to 15% true strain.

²K-value is the magnitude of true stress extrapolated to a true strain of 1.0. It is a material property parameter frequently used by one-step forming simulation codes.

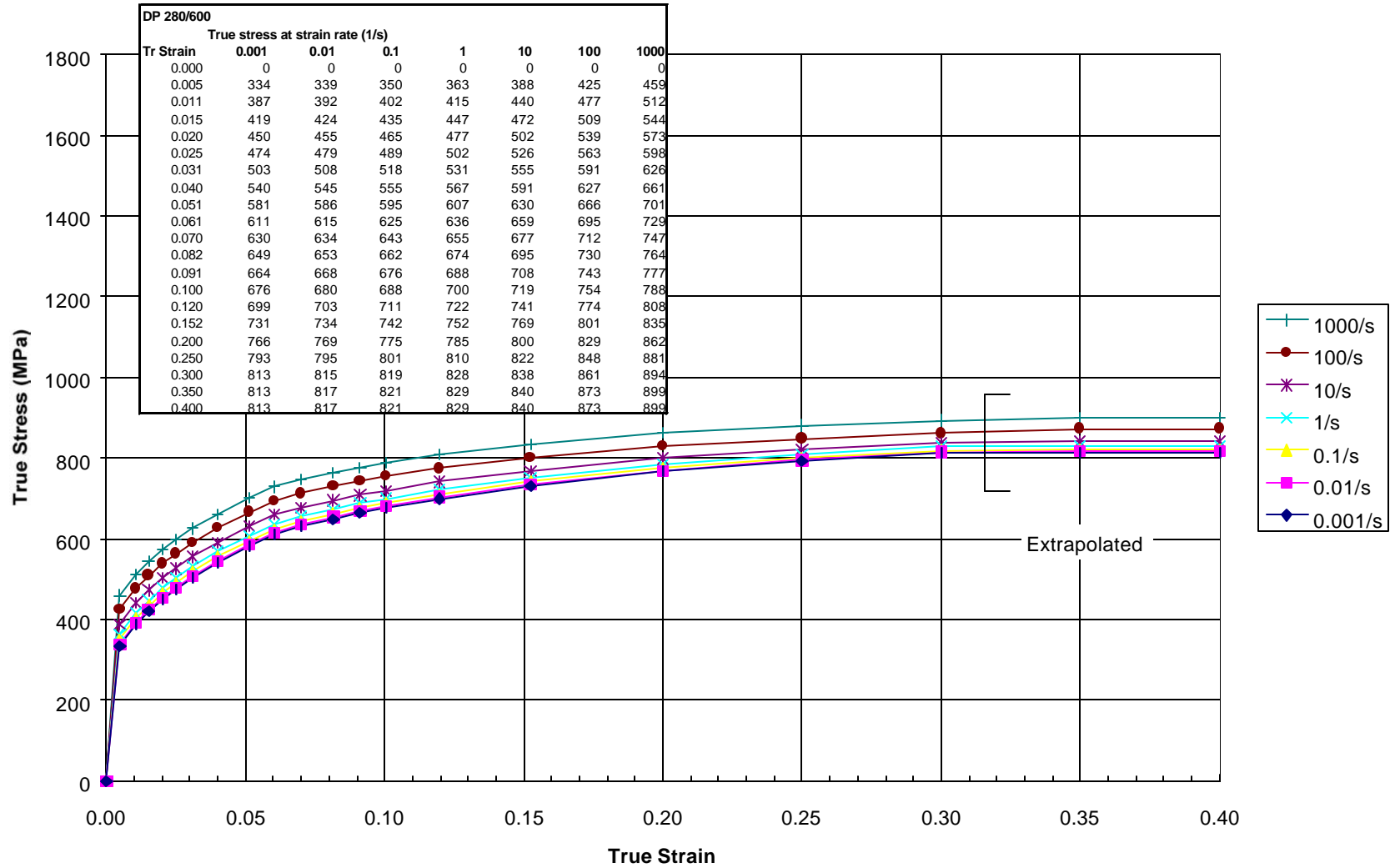
BH 210/340

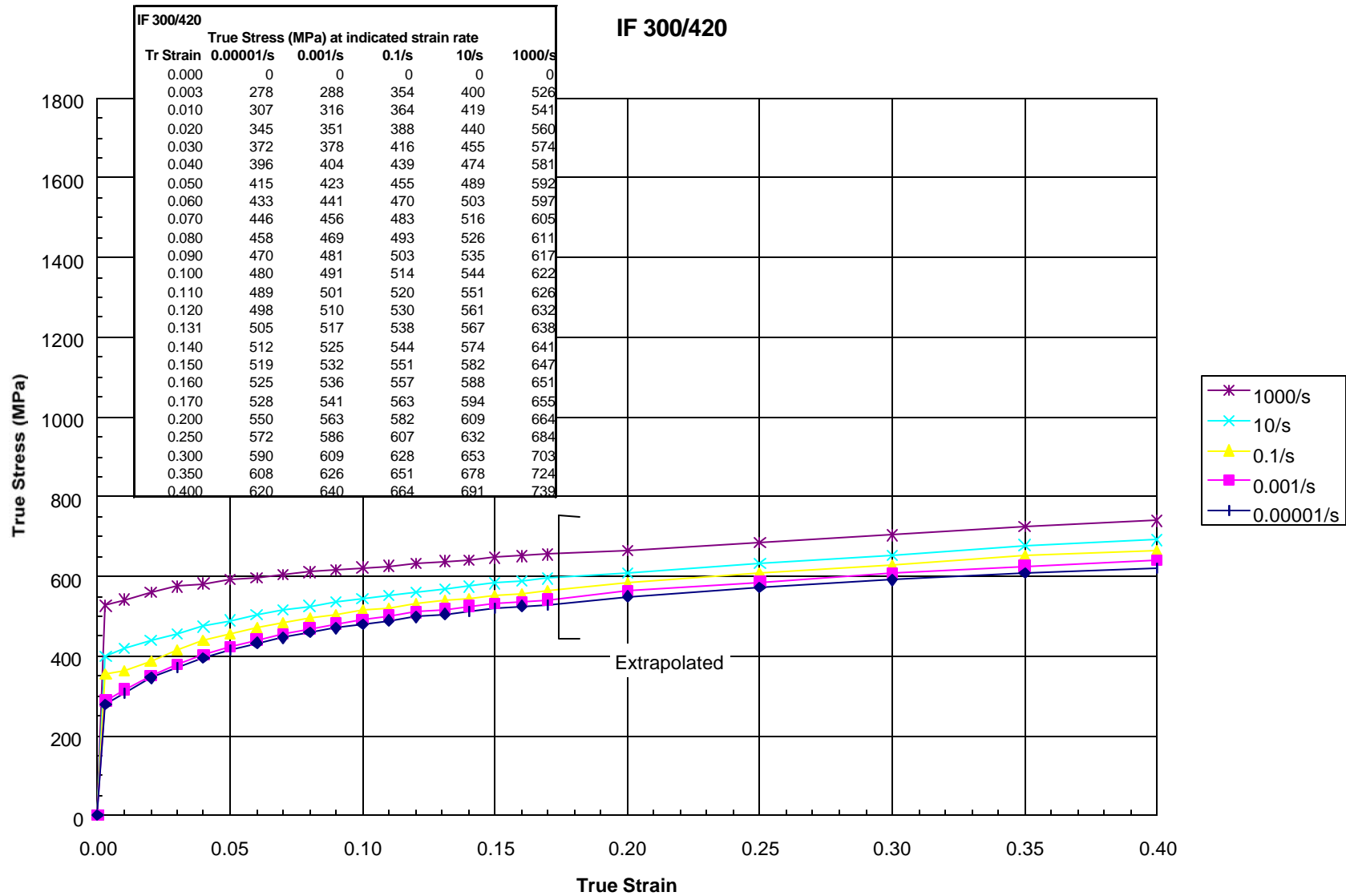


BH 260/370

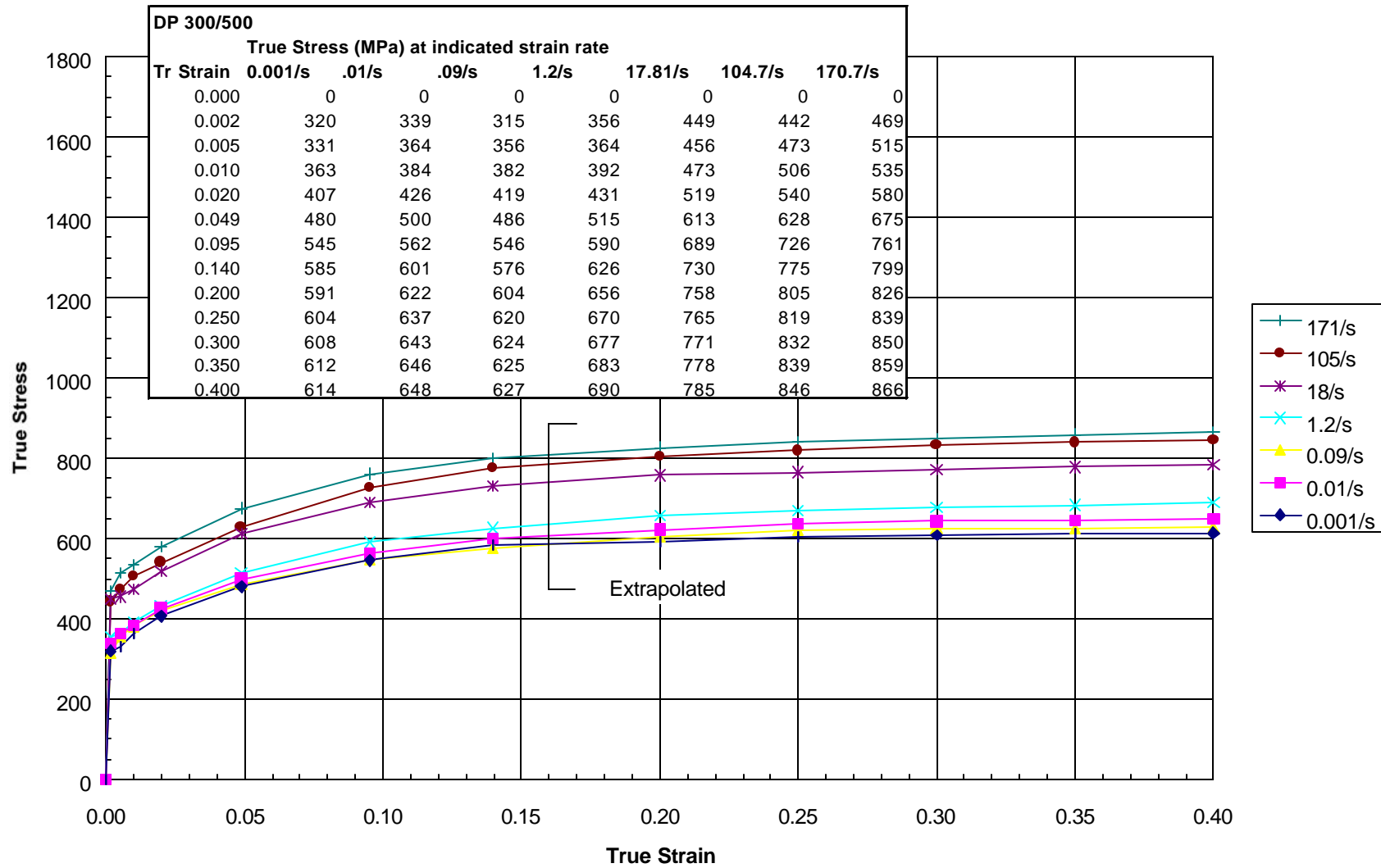


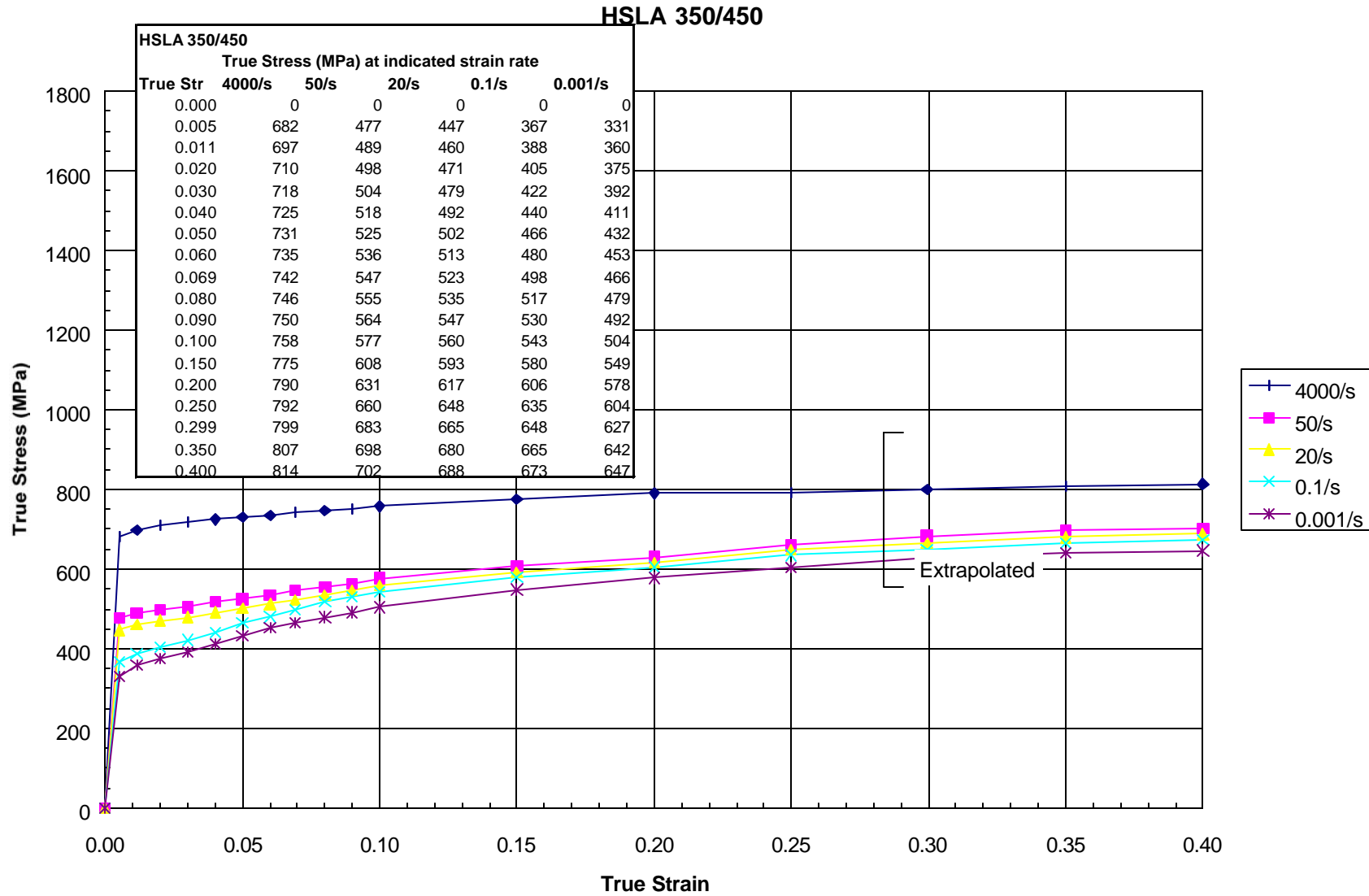
DP 280/600

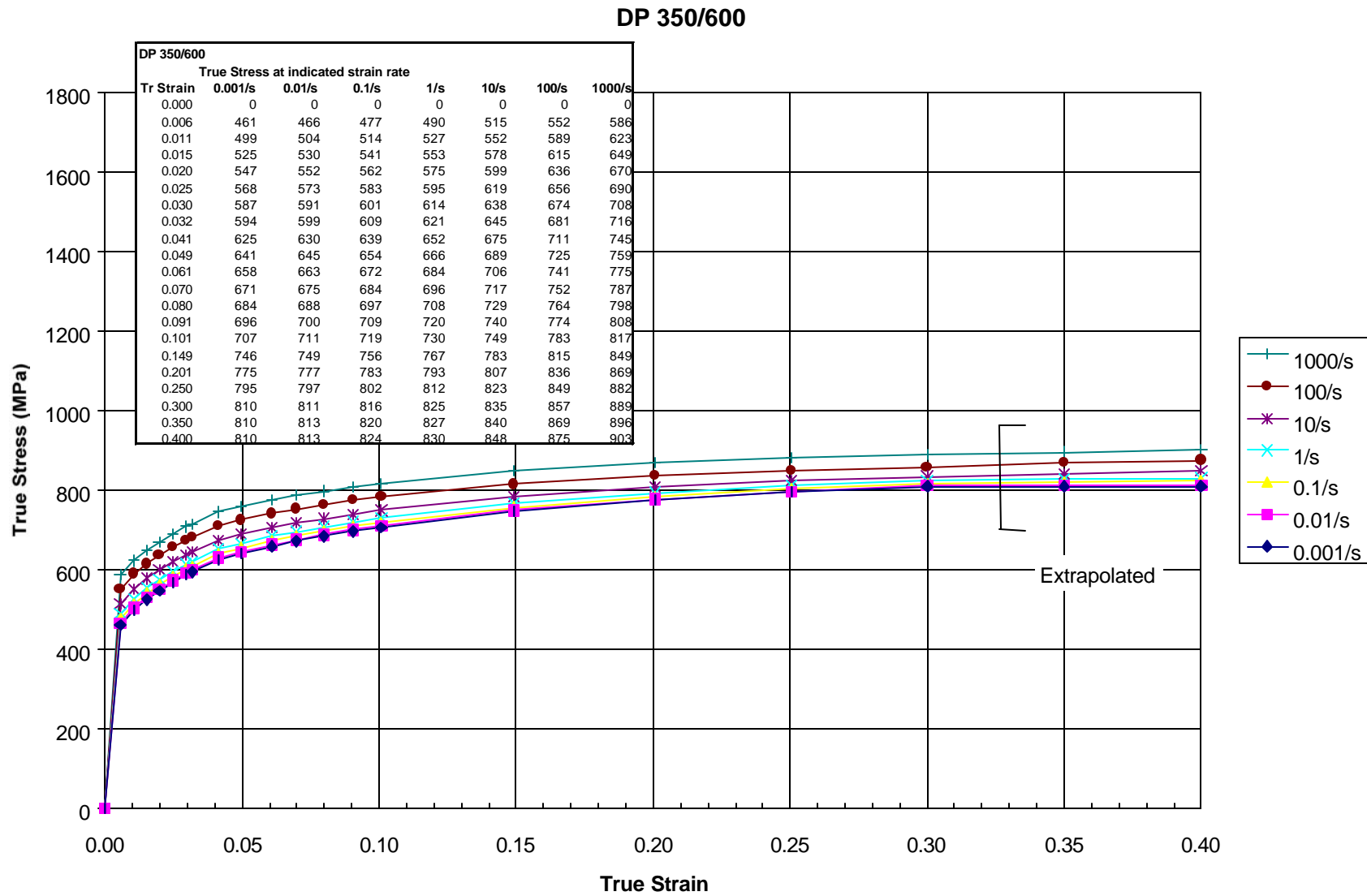


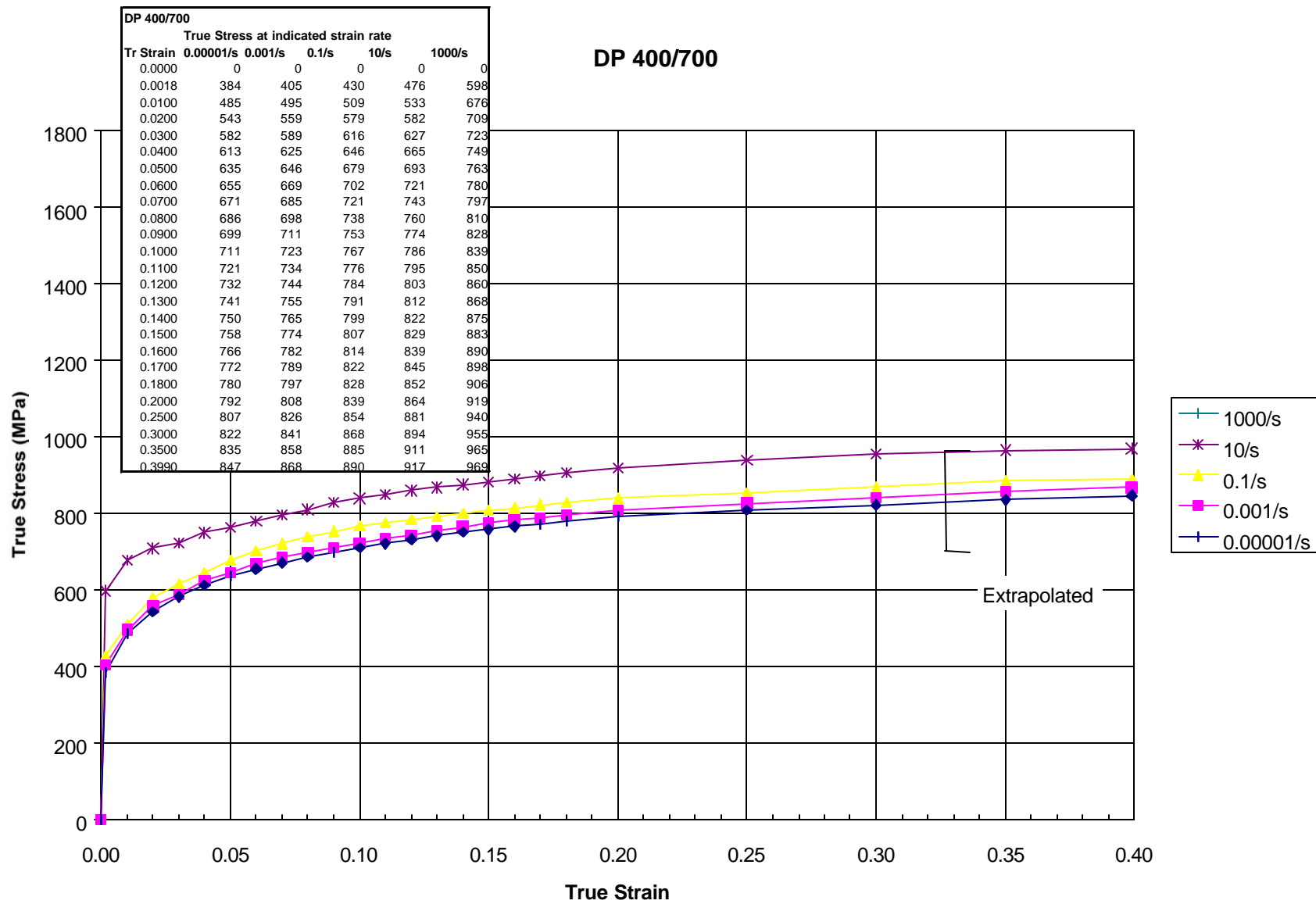


DP 300/500

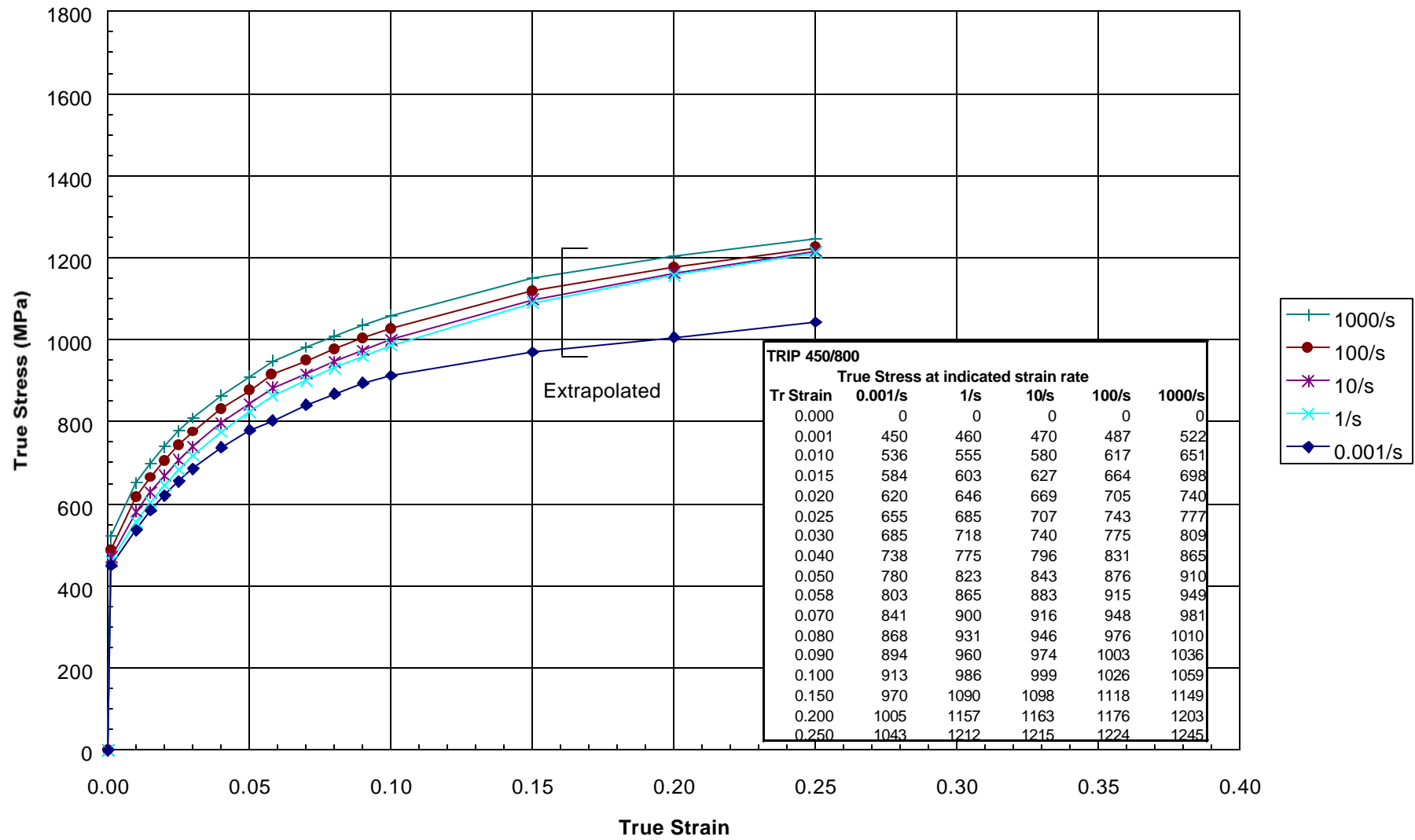




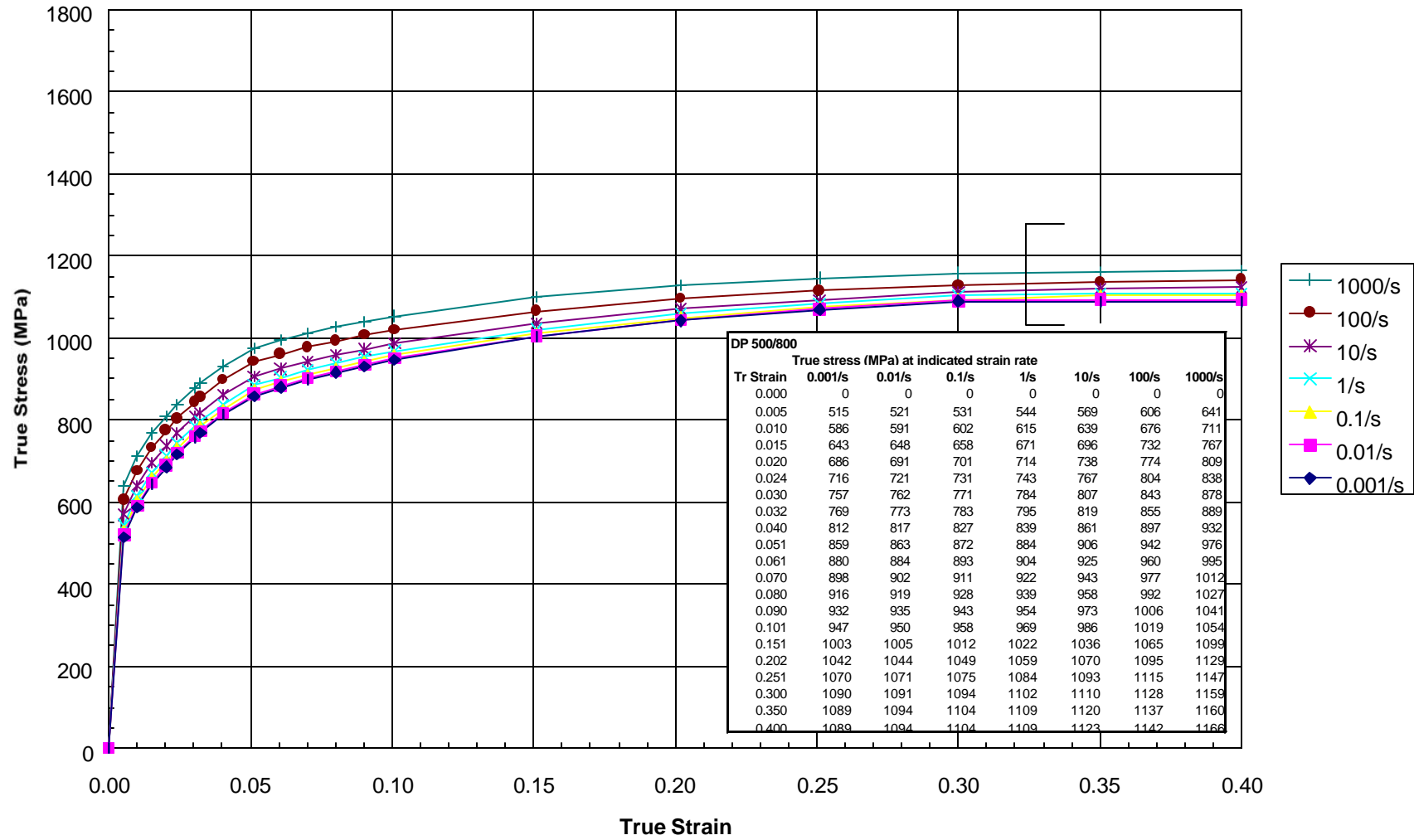




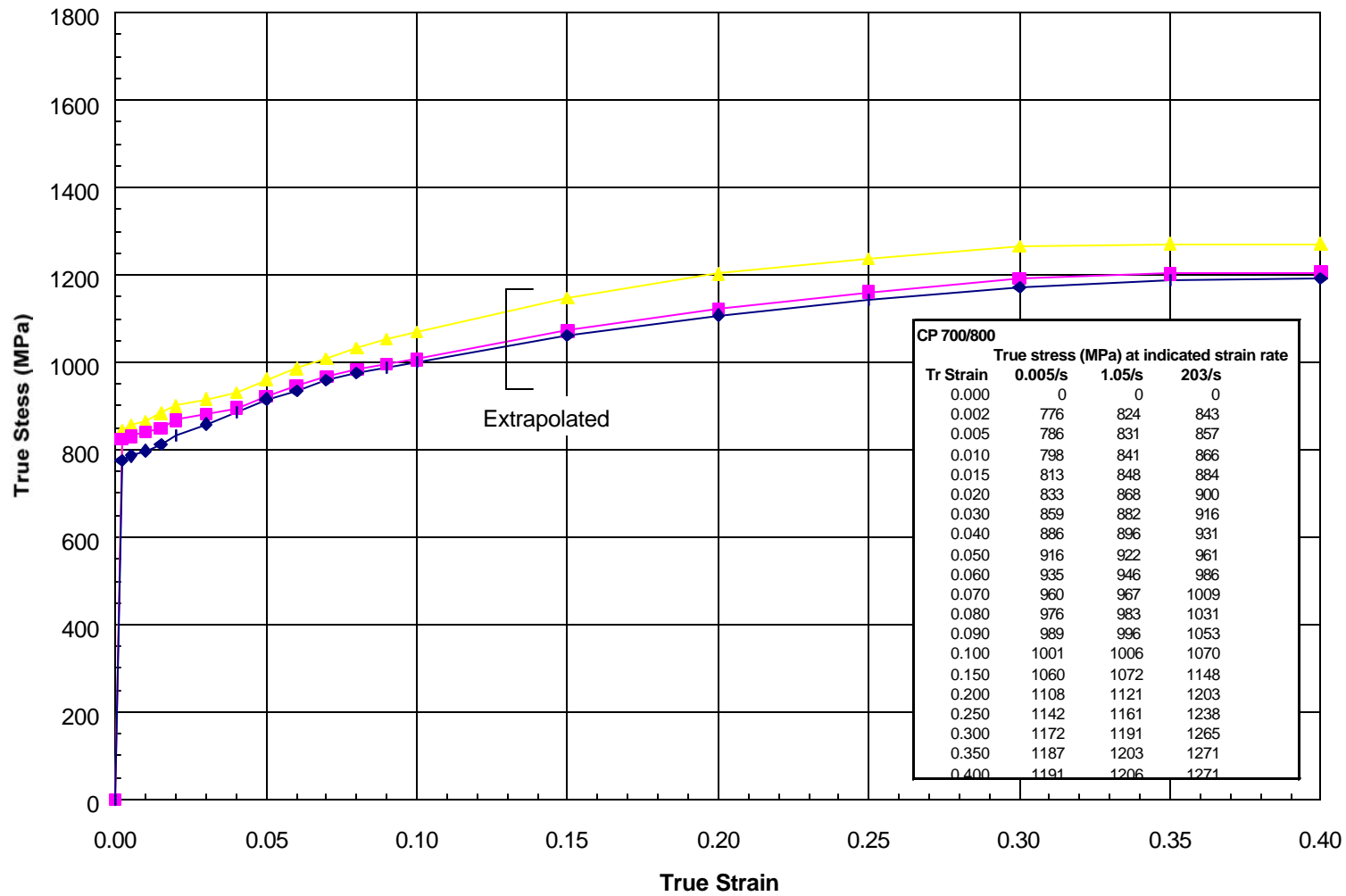
TRIP 450/800



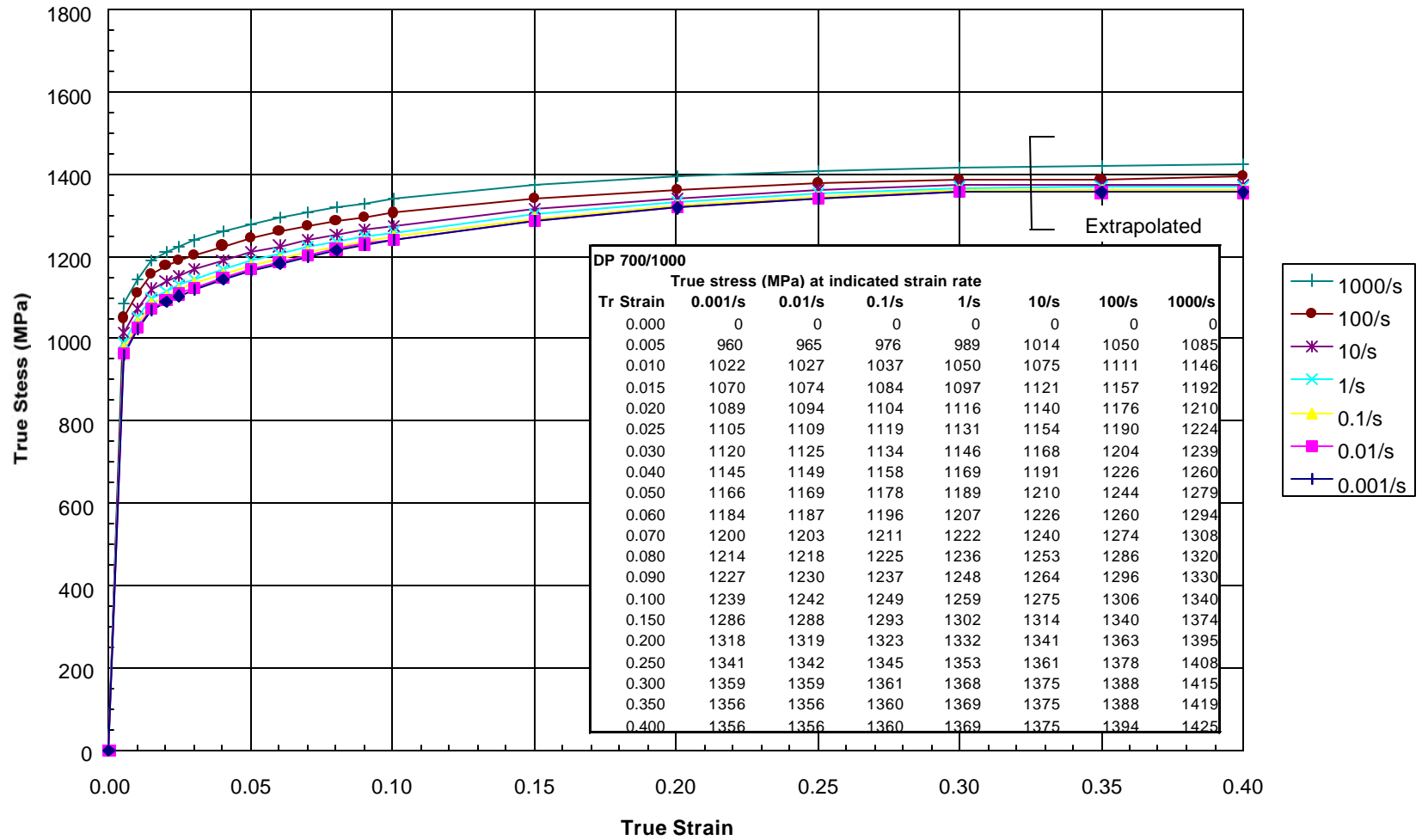
DP 500/800



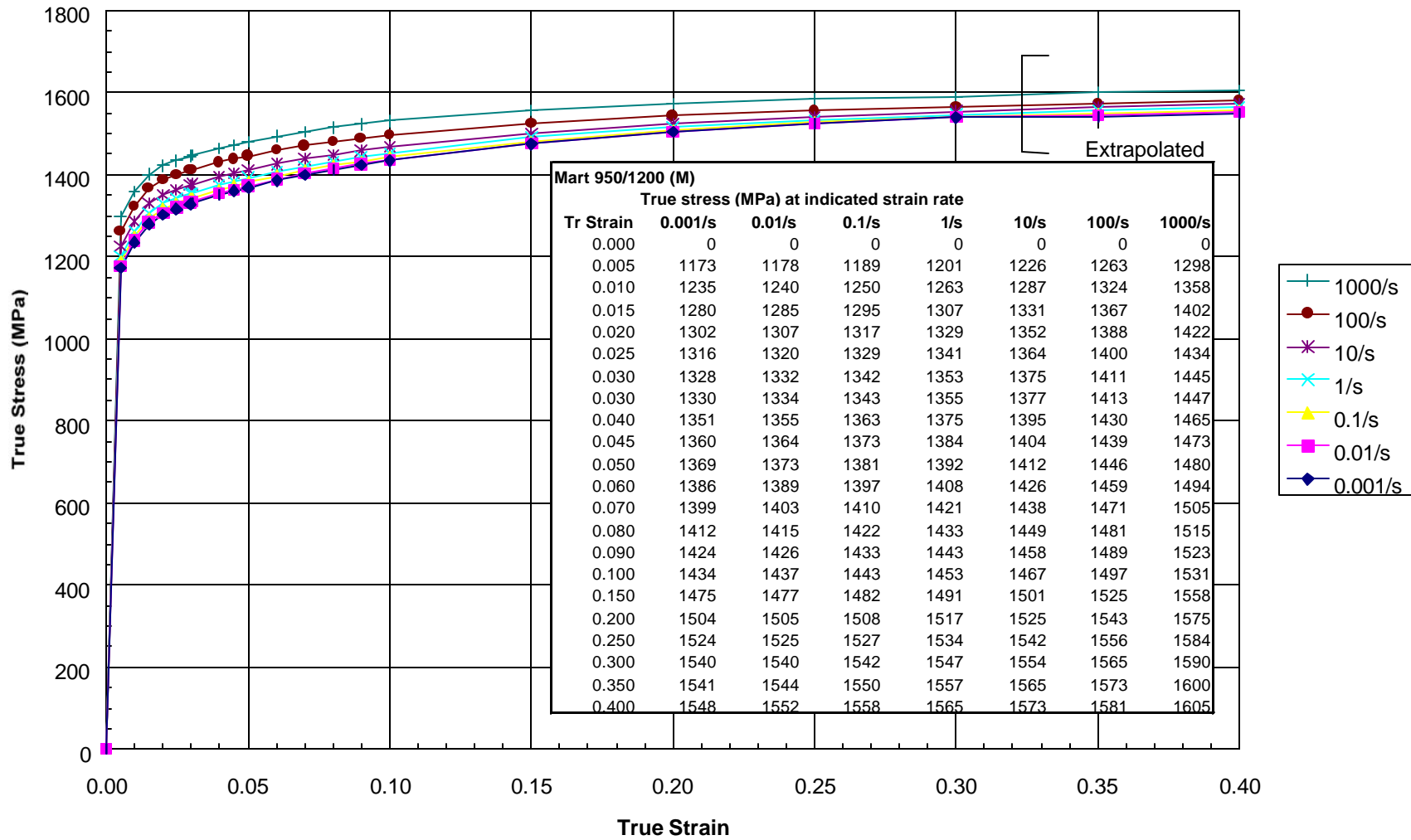
CP 700/800



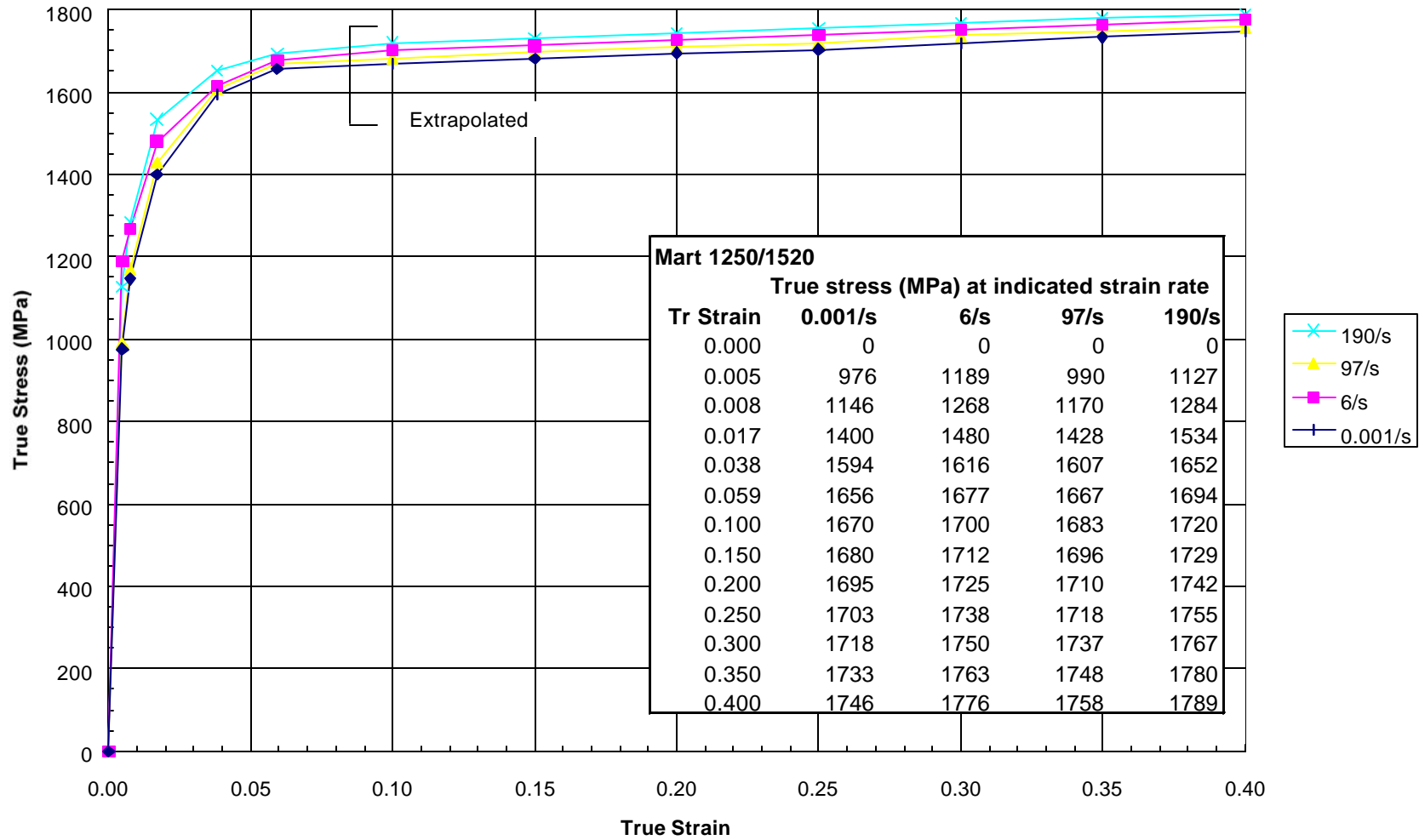
DP 700/1000



Mart 950/1200



Mart 1250/1520



**ULSAB-AVC
Advanced Vehicle Concepts**

Technical transfer Dispatch #6 (TTD6)

**Appendix III - Considerations in the Selection of
Advanced High Strength Steels for ULSAB-AVC**

Considerations in the Selection of Advanced High Strength Steels for ULSAB-AVC

General Principles

The principal difference between Advanced High Strength Steels (AHSS), based on the multi-phase concept, and conventional High Strength Low Alloy (HSLA) steels is the higher strain, or work, hardening capacity of AHSS. This behaviour can provide significant benefits in both component manufacture and performance.

A high work hardening capacity positively influences formability by resisting local necking during component manufacture and is especially important in the stretch forming deformation modes typically encountered in the manufacture of many automotive body components. High work hardening capacities also result in higher ultimate tensile strengths (UTS) in the manufactured component, which enhances crash energy absorption and fatigue performance. In multiphase steels, the as-manufactured yield strength is enhanced by bake-hardening effects, which increase with increasing forming strain (1). Unlike conventional BH steels, which attain a somewhat constant value of bake hardening after work hardening of 1~2%. This increase in YS enhances the anti-denting performance.

When deformed at ambient temperature, the flow stresses of conventional steels show positive strain rate dependence. That is, higher rates of deformation result in increased strength levels. This behaviour persists with multiphase steels. The static (10^{-3} s^{-1}) and dynamic (10^2 s^{-1}) tensile strengths of the steels for ULSAB-AVC were estimated from their true stress-true strain curves. The increment in UTS when strain rate increased from 10^{-3} s^{-1} to 10^2 s^{-1} was generally constant, in the range of 80 to 110 MPa, independent of both strength and microstructure. The ratio of dynamic to static UTS is shown as a function of static UTS in Figure 1. At elevated strain rates, the strength of both conventional and multi-phase steels is dramatically enhanced.

In Figure 2, the static (10^{-3} s^{-1}) and dynamic (10^2 s^{-1}) tensile strengths of three steels used in the ULSAB-AVC are compared. In this example, the dual phase steels provide substantial tensile strength advantage over the HSLA product under both static and dynamic deformation conditions.

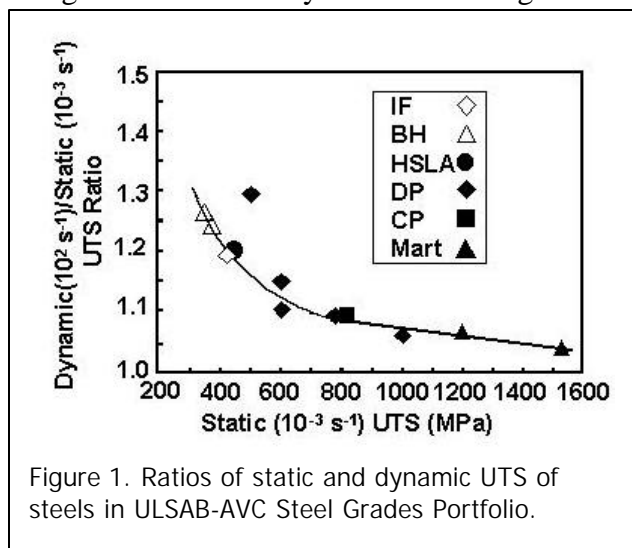


Figure 1. Ratios of static and dynamic UTS of steels in ULSAB-AVC Steel Grades Portfolio.

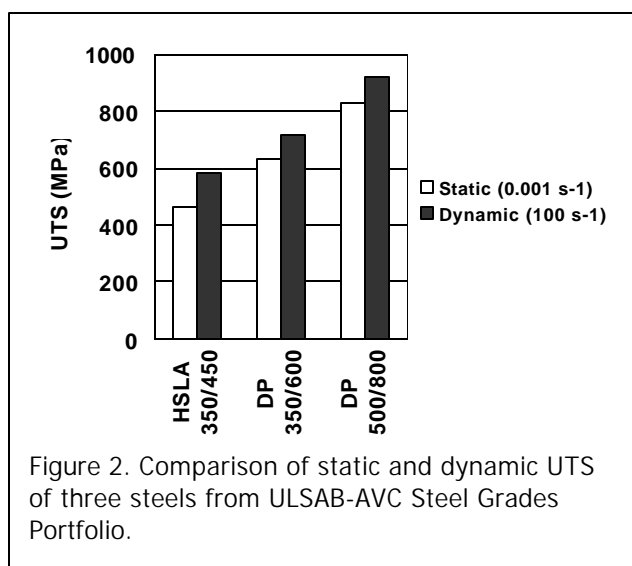


Figure 2. Comparison of static and dynamic UTS of three steels from ULSAB-AVC Steel Grades Portfolio.

ULSAB crashworthiness simulations used static mechanical properties and relied on model tuning factors to match predictions to physical crash results. The ULSAB-AVC steel producers provided dynamic mechanical properties for use in computer crash simulations. Dynamic mechanical properties provide better prediction of load path, better prediction of plastic instability during collapse, and eliminate the need for some artificial tuning constants (2-4). These aspects are, of course, examined in the ULSAB-AVC Program.

During a crash event, energy is absorbed by plastic deformation of the key structural components. The absorbed energy is related to collapse load (flow stress) and total strain imparted by the crash and can be estimated by the area under the stress-strain curve at specific levels of strain. Studies to determine these specific strain levels, and the strain rate, during typical vehicle crashes have shown that the majority of the energy is absorbed at plastic strains of up to 10% and strain rates between $100 \sim 300 \text{ s}^{-1}$ (5). In Figure 3 (6), energy absorbed at 10% strain during dynamic deformation of conventional and AHSS products of three yield strength levels are compared. Under the conditions of strain and strain rate typically encountered in a crash, the AHSS absorb more energy. It is therefore proposed that initial steel selection for crash-sensitive applications be made on the basis of area under the stress strain curve at 10% plastic strain, measured at strain rates of $100\text{-}300 \text{ s}^{-1}$.

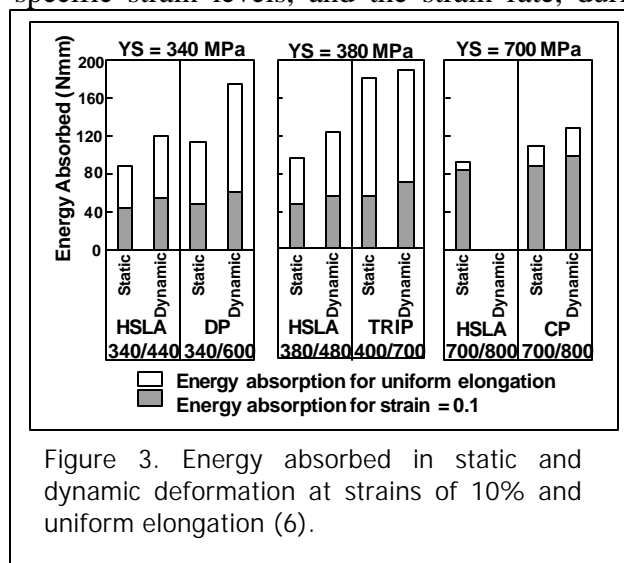


Figure 3. Energy absorbed in static and dynamic deformation at strains of 10% and uniform elongation (6).

Crash Energy Absorption

As already shown in ULSAB, the primary factors controlling the static bending and torsion performance of the automobile body structure are section design, gauge, and elastic modulus. These factors are independent of the material strength level and microstructure. However, designers must also ensure that working stresses do not exceed the yield strength of the material. Therefore, Advanced High Strength Steels potentially provide a significant lightweighting opportunity by avoiding the need to use heavier-gauge materials for applications where gauge is limited by maximum working stress rather than by elastic deformation. This is particularly important for those components that take part in crash energy management.

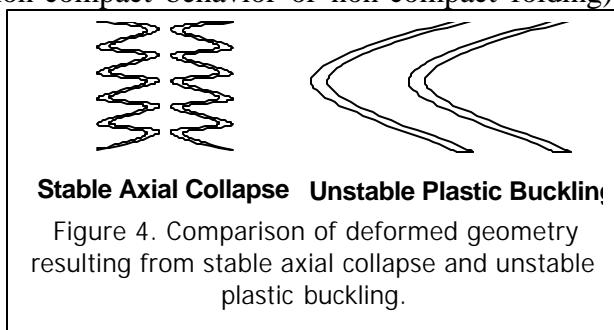
The ULSAB-AVC body structure is designed to absorb crash energy so that the magnitude of both peak decelerations and intrusion into the passenger compartment are minimized. In these considerations, material mechanical properties and work hardening characteristics become extremely important and advanced high strength steels offer key advantages.

In longitudinally loaded components, such as front and rear rails (in front or rear impact) and cross members (in side impact), maximum energy is absorbed when stable progressive axial

collapse (also called compact behavior or compact folding) is maintained. Increasing either the volume of material deformed or the energy under the material's stress-strain curve will increase the absorbed energy. The higher work hardening capacity of AHSS provides for improvements compared with conventional high strength steels of equivalent yield strength, in both respects. The higher work-hardening distributes strain more uniformly, involving a greater volume of material in the deformation event, and the greater area under the stress-strain curve (for equivalent starting yield strength) absorbs greater total energy for a given degree of deformation. While similar performance could be provided by conventional high strength steel with similar UTS levels, the greater formability of AHSS permits their use in applications that would preclude using the less formable conventional HSS.

To provide high crash energy absorption, front and rear end components must resist deformation by less efficient plastic buckling (also called non-compact behavior or non-compact folding).

This requirement is illustrated in Figure 4, which compares the geometry of sections that deform by stable axial collapse and unstable plastic buckling. The section that deformed by stable axial collapse contains a greater number of regular folds, involves a greater volume of material in the deformation event, and absorbs greater energy for a fixed collapse length. Stable axial collapse is promoted by increasing yield strength, increasing the ratio of thickness to column width (a geometry factor), increasing strain hardening rate, and decreasing the angle between direction of loading and axis of component (7).



For components properly designed to deform by stable axial collapse, dynamic behavior during collapse of thin wall rectangular columns is frequently described by equations of the form:

$$P_m = K\sigma^a \quad (\text{Equation 1})$$

where P_m = average load (or absorbed energy),
 K = constant related to geometry,
 σ = flow stress term,
 t = thickness, and
 a = thickness exponent.

Studies of impact deformation of square columns (8) found Equation 1 described experimental absorbed energy at 150 mm deformation when $\sigma = (\sigma_{\text{uts}})^{0.506}$ and $a = 1.498$. More recent studies of axial collapse of closed top hat structures made of conventional and dual phase steels of varying thicknesses have been performed. (9) These studies concluded that Equation 1 described experimental mean collapse load at 48 km/h when $\sigma = (\sigma_{\text{uts}})^{0.4}$, in good agreement with reference (8), but the thickness exponent, a , ranged from 1.6 to 2.0 depending on steel grade, geometry, and deformation conditions. In both studies, it was pointed out that the equations are valid only for stable axial collapse for the specific geometry and deformation conditions investigated.

While further study is required to fully explain the combined effects of steel grade, strength, gauge, geometry, and deformation conditions on crash performance, Equation 1 begins to demonstrate the profound effect of gauge on crash energy absorption. Figure 5 was generated by substituting $(\sigma_{\text{uts}})^{0.4}$ for σ and setting $a=1.8$ in Equation 1 and plotting UTS and thickness for several constant values of Pm/K . It illustrates the UTS required to maintain constant crash load as thickness changes. This plot is similar to plots of yield strength and gauge required to maintain constant crash energy absorption of other investigations (5). Using this same form of Equation 1 (substituting $(\sigma_{\text{uts}})^{0.4}$ for σ and setting $a=1.8$), the data of Figure 6 shows the relative increases in UTS required to decrease gauge (mass) while maintaining constant average crash load or energy absorption. Figures 5 and 6 demonstrate that in the absence of geometry changes, exponentially greater increases in UTS are required to maintain constant energy absorption as gauge is reduced. This sets a practical upper limit for the degree to which mass can be reduced by substituting lighter gauge, higher strength materials. Substantial mass reductions in critical crash energy management components can only be achieved when geometry is optimized to take full advantage of the unique mechanical properties of AHSS. Efficient design must therefore be a primary emphasis for reducing mass while maintaining or improving crash performance.

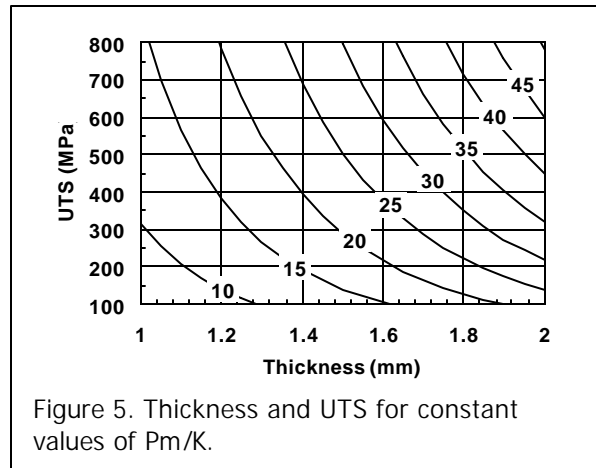


Figure 5. Thickness and UTS for constant values of Pm/K .

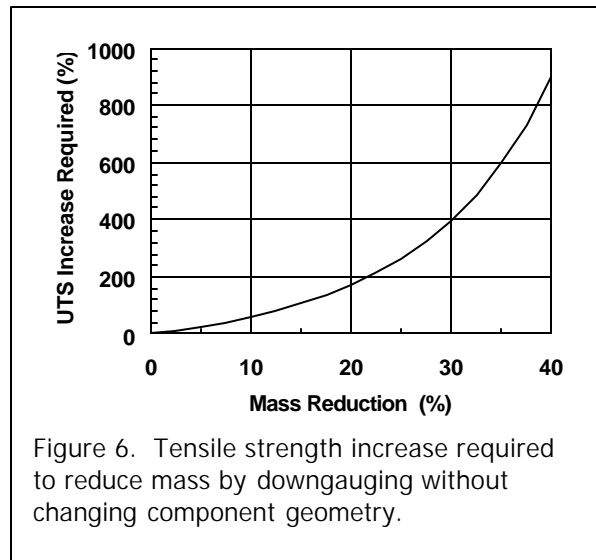


Figure 6. Tensile strength increase required to reduce mass by downgauging without changing component geometry.

For ULSAB-AVC transversely loaded components, such as rockers, pillars, and roof rails in side impact, resistance to plastic bending is a significant consideration. In these applications, high yield strength and high work hardening rate are of great importance. The higher strength multi-phase steels should excel in these applications as their excellent formability permits the use of higher yield strength products for components that could not be formed with conventional HSS.

Dent Resistance

Dent resistance is primarily a factor in outer body panel applications. Strength, gauge, panel curvature, and panel stiffness influence dent resistance. A general guideline (10) for assessing dent resistance is:

$$P_{0.1} \sim A \sigma_y t^n \quad (\text{Equation 2})$$

where $P_{0.1}$ = load to produce 0.1 mm deep dent,
 A = constant which accounts for geometry and panel stiffness effects,
 σ_y = yield strength after 2% strain and paint bake,
 t = as-formed panel thickness, and
 n = 2.0-2.4 depending on overall panel stiffness.

While this equation is useful for comparing the relative dent resistances of similar types of materials with different strength levels, care must be used when comparing materials of differing strengthening mechanisms. Yield strength is normally measured by the 0.2% offset method. FEA forming simulations (11) of strains in the vicinity of 0.1 mm deep dents found peak strain to be on the order of only about 0.1%. Initially, the excellent dent resistance of conventional bake hardenable steels was attributed to the return of a sharp upper yield point after strain and paint baking, since these materials will remain elastic at larger stresses than those which demonstrate continuous yielding. Unfortunately, attempts to correlate dent resistance to yield point measured at strains below 0.2% have not been successful (12). Furthermore, multi-phase steels show strong bake hardening and provide excellent dent resistance without a sharp yield point after strain and paint baking.

Dent load data (13) from the ULSAC prototype door project also suggest that factors other than yield strength and thickness affect dent resistance. The dent load required to produce an observable dent is shown as a function of in-panel yield strength in Figure 7.

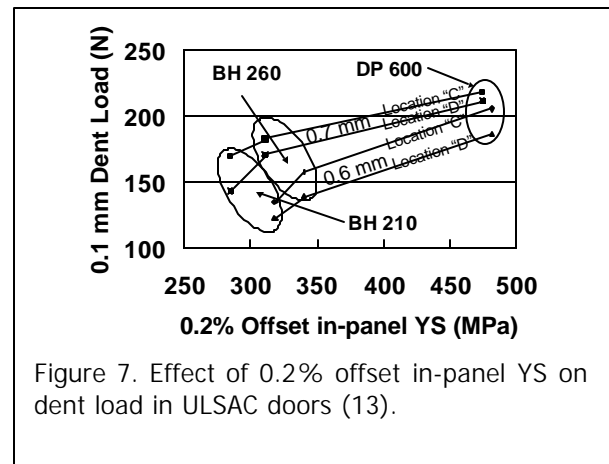


Figure 7. Effect of 0.2% offset in-panel YS on dent load in ULSAC doors (13).

Fatigue

Excellent durability is, of course, a prerequisite consideration for vehicle design. Advanced High Strength Steels enable optimal fatigue performance to be achieved because they allow higher working stresses to be accommodated. To achieve this optimum requires that the design and manufacturing methods for the auto body structure be adjusted to match the higher working stresses allowable.

The fatigue strength of un-notched or mildly notched base material increases with increasing tensile properties of the steel. This is illustrated by the data of Figure 8 (uniaxial tension-tension, 14, 15) which shows the excellent fatigue performance. Fatigue endurance limit continues to increase with increasing tensile strength in these steels. Strain hardening and bake hardening improve fatigue endurance limit, Figure 9 (16).

For mechanically notched material such as punched holes, reversed plastic strains appear in the notch even if the nominal stress away from the notch is elastic. Investigations (16) have shown that due to cyclic softening there is little, or no effect, of strain hardening if the yield to tensile ratio exceeds 0.7-0.75.

Fatigue of spot welds can be a limiting factor for body structure endurance. Inherent natural defects are present in welds and the fatigue process is governed by crack propagation; resistance to crack growth is generally independent of tensile strength. For load carrying welds there is little or no effect of increased base metal tensile strength and consequently no effect of strain- or bake hardening. Decreasing spot pitch (increasing the number of welds) or increasing spot weld diameter can compensate for this. The most rational compensation, however, to use weld bonding or continuous welds in fatigue-critical areas.

ULSAB-AVC Design Evolution Methodology

Multi-phase Advanced High Strength Steels used in the ULSAB-AVC vehicle offer superior strength, formability, and crash energy absorption capacity and provide very good dent resistance and fatigue performance. These steels provide exceptional potential for increased structural strength and mass reduction by using lighter thickness than could be used with less formable conventional steel. When selecting AHSS for ULSAB-AVC, the following guidelines were applied.

- The steel selection for crash-sensitive applications was made utilizing the area under the stress-strain curve at 10% strain, measured at strain rates from 100 ~300s⁻¹.

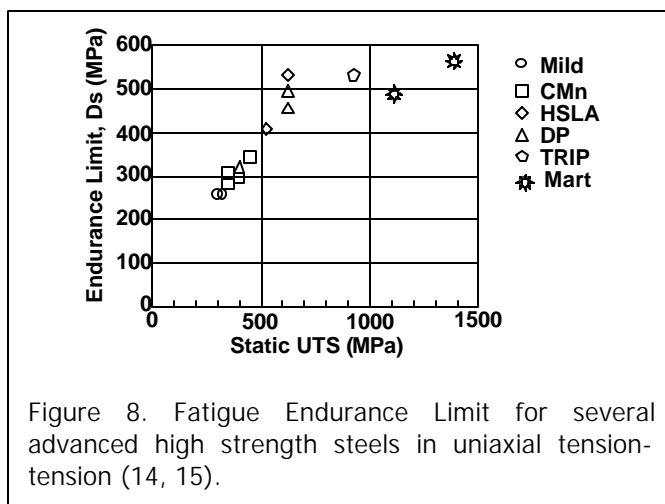


Figure 8. Fatigue Endurance Limit for several advanced high strength steels in uniaxial tension-tension (14, 15).

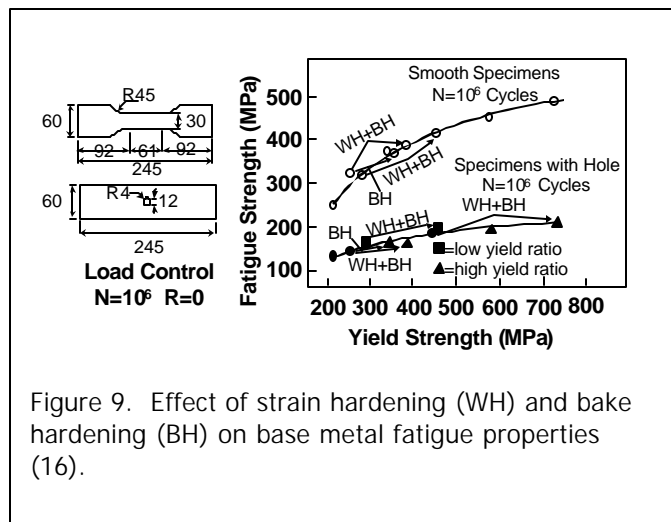


Figure 9. Effect of strain hardening (WH) and bake hardening (BH) on base metal fatigue properties (16).

- Designing components in AHSS was performed so that the as-manufactured strength in the component was maximized by strain hardening, consistent with formability and thinning considerations.
- Strength comparisons were made at strain rates that reflect those experienced.
- For constant component geometry (i.e. no structural design changes) exponentially greater increases in strength are required to maintain crash energy absorption capacity as thickness decreases, limiting the extent to which mass can be reduced by substituting higher strength, lighter gauge materials. Component design (geometry or shape) was the primary initial focus for achieving the best result in reducing mass while maintaining or enhancing crash performance in ULSAB-AVC.

There is a high degree of complexity and a strong interaction between component design and materials selection inherent in the development of advanced lightweight vehicles like ULSAB-AVC. Therefore, the design and materials teams worked closely throughout the design process to assure that design was optimized and that the steels selected, either conventional or AHSS, were to their full potential. To assure the ULSAB-AVC takes full advantage of conventional and advanced steels, the following design methodology was applied:

For each component that is not limited by elastic modulus, the ULSAB-AVC static bending and torsion requirements were addressed using the lightest gauge, highest strength AHSS that simultaneously met stiffness, working stress, and formability requirements. Here, FEA forming simulations were used not only to verify forming feasibility but also to document in-part strength and gauge to determine if additional gauge reductions were possible. This process was carried out within the holistic, iterative design process so that changes in one component did not adversely affect stresses and deflections in other components.

When designing for crash performance, ULSAB-AVC crash model simulations used dynamic as-produced mechanical properties at minimum specified strength and gauge in the first design step unless forming simulation results were available to provide as-formed properties and gauge. If crash targets were not met in initial iterations, higher strength advanced steels were substituted first to determine if crash energy management can be improved without adding gauge. Candidates for substitution were selected by comparing energy under the stress-strain curve at 10% strain for minimum strength level products tested at a strain rate of 100-300 s⁻¹. As in the case of static design, components designed with AHSS for crash considerations were subjected to forming simulations to verify forming feasibility. Gauge increases were not considered until it was established that there was no higher strength product available to form the part successfully after redesign and meet both static and dynamic performance requirements.

In summary, the selection of steels for ULSAB-AVC was made to facilitate an optimum balance between structural strength, crash resistance, formability, joinability and total economy to meet credibly achieve the ULSAB-AVC technical goals. Clearly, this could only be obtained through Simultaneous Engineering between the material suppliers and vehicle designers.

References

1. B. Engl, "New Steel Concepts Match Up to the Challenge by Lighter Weight Constructions," Proceedings, EUROMAT, Munich, September 1999.
2. S. Simunovic and J. Shaw, "Effect of Strain Rate and Material Processing in Full Vehicle Crash Analysis," SAE Technical Paper No. 2000-01-2715, Society of Automotive Engineers, Warrendale, PA, USA.
3. "Strain Rate Dependent Steel Material Properties in CAE Analysis for Crashworthiness," Porsche Engineering Services Report to ULSAB-AVC Consortium, April, 2000
4. K. Mahadevan, P. Liang, and J. R. Fekete, "Effect of Strain Rate in Full Vehicle Frontal Crash Analysis," SAE Technical Paper no. 2000-01-0625, Society of Automotive Engineers, Warrendale, PA, USA
5. K. Sato, A. Yoshitake, Y. Hosoya, and T. Yokoyama, "A Study On Improving The Crashworthiness Of Automotive Parts By Using Hat Square Columns," Proceedings, IBEC, Vol. 31 - Interior, Safety, & Environment, 1997, Warren, MI, USA
6. B. Engl and E.-J. Drewes, "New High Strength Steels with Good Formability for Automotive Applications," ATS Conference, Paris, December 2000, to be published in *Revue de Metallurgie*.
7. A. Uenishi, Y. Kuriyama, M. Usuda, M. Suehiro, "Improvement Of Crashworthiness By Application Of High Strength Steel For Light Weight Auto Bodies," Proceedings, IBEC '97, Auto Body Materials, 1997, Warren, MI, USA, pp. 59-66.
8. J. O. Sperle and H. Lundh, "Strength and crash resistance of structural members in high strength dual phase steels," *Skand. J. of Metal.*, 13, pp. 343-351, 1984.
9. M. Marsh, "Development of AutoBody Sheet Materials for Crash Performance," conference on "Materials & Structures for Energy Absorption," IMechE, London, May 9, 2000.
10. Y. Yutori, S. Nomura, I. Kokubo, and H. Ishigaki, "Studies on the Static Dent Resistance," Proceedings of the 11th IDDRG, *Les Memoires Sci. Rev. Met.*, 1980, pp. 561-569 (1980)
11. S. Sadagopan, "Applications of Computer Modeling to the Analysis of Frictional Behavior, Formability, and Performance of Sheet Steel," Colorado School of Mines Advanced Steel Processing and Properties Research Center Report No. MT-SRC-098-020, Section 7.0, September, (1998).
12. B. J. Allen, D. K. Matlock, S. Sadagopan, and J. G. Speer, "The Effects of Flow Stress on the Dent Resistance Performance of Sheet Steels," Proceedings, 40th MWSP Conference, Vol. XXXVI, Iron and Steel Society, Warrendale, PA, (1998), 83-92
13. Porsche Engineering Services, Inc., "ULSAC Engineering Report," Final report to Ultra-Light Steel Auto Closures Consortium, April, 2000.
14. "High Strength Steels for Automobiles", Technical Bulletin No. 243-116-01, NKK Corporation, Tokyo, (1995), p. 50.
15. K. Eberle, Ph. Harlet, P. Cantineaus, and M. Vande Populiere, "New thermomechanical strategies for the realization of multiphase steels showing a transformation induced plasticity (TRIP) effect," 40th MWSP Conference, Vol. XXXVI, Iron and Steel Society, Warrendale, PA, (1998), 83-92
16. J.-O. Sperle, "Fatigue Strength of High Strength Dual-Phase Steel Sheet," *Int. Journal of Fatigue* 7 no 2 (1985) pp. 79-86.

**ULSAB-AVC
Advanced Vehicle Concepts**

Technical transfer Dispatch #6 (TTD6)

Appendix IV - Examples of ULSAB-AVC FEA forming simulations

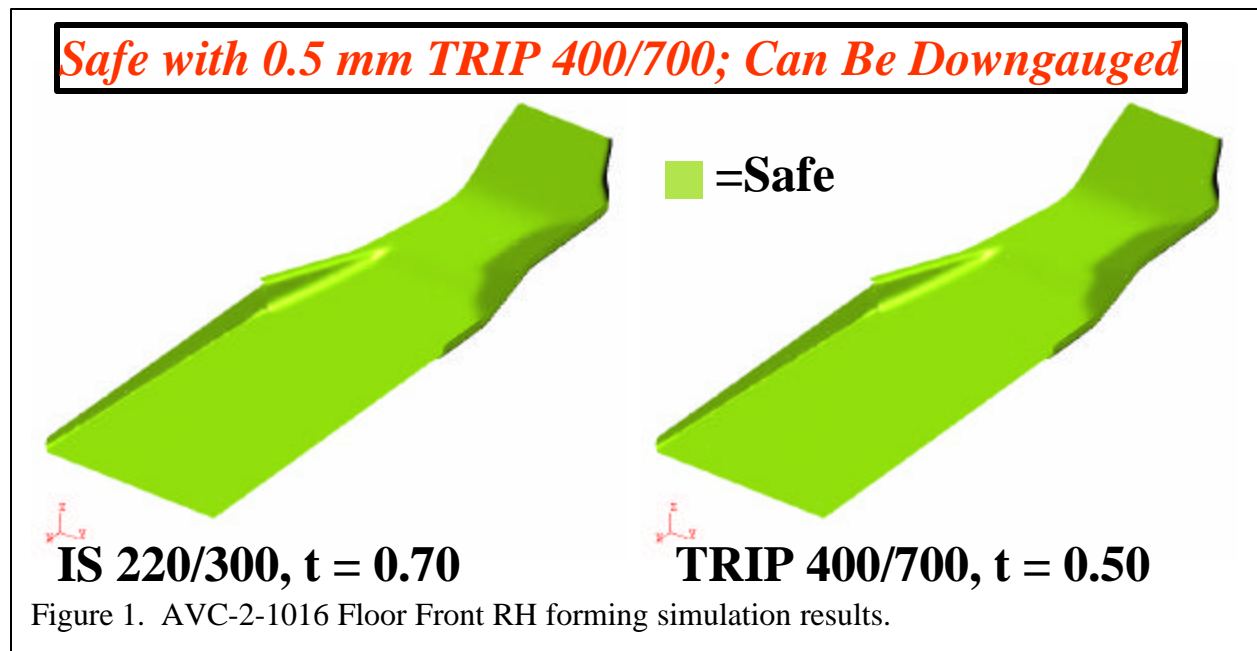
Examples of ULSAB-AVC FEA Forming Simulations.

All major ULSAB-AVC body structure components were analyzed using one-step forming FEA to assess the likely forming behavior early in the concept design process. A total of 126 parts were analyzed. For those parts where critical strains were predicted in the initial forming feasibility review, changes in material or geometry were iteratively reviewed with PES until concept designs with acceptable behavior were obtained. As components were modified to achieve design goals, additional forming simulations were only performed when it was felt that the component design had changed sufficiently to render the initial forming simulation results invalid. At the conclusion of the body structure component design process, all parts were considered to show acceptable forming behavior.

Selected examples of one-step FEA forming simulations are provided in this appendix. These demonstrate how forming simulations were used to identify opportunities to replace expensive forming processes with less expensive stampings; to identify components with low forming strains, and, therefore, become candidates for down-gauging with higher strength grades, and also to resolve forming problems by recommending grade and geometry modifications.

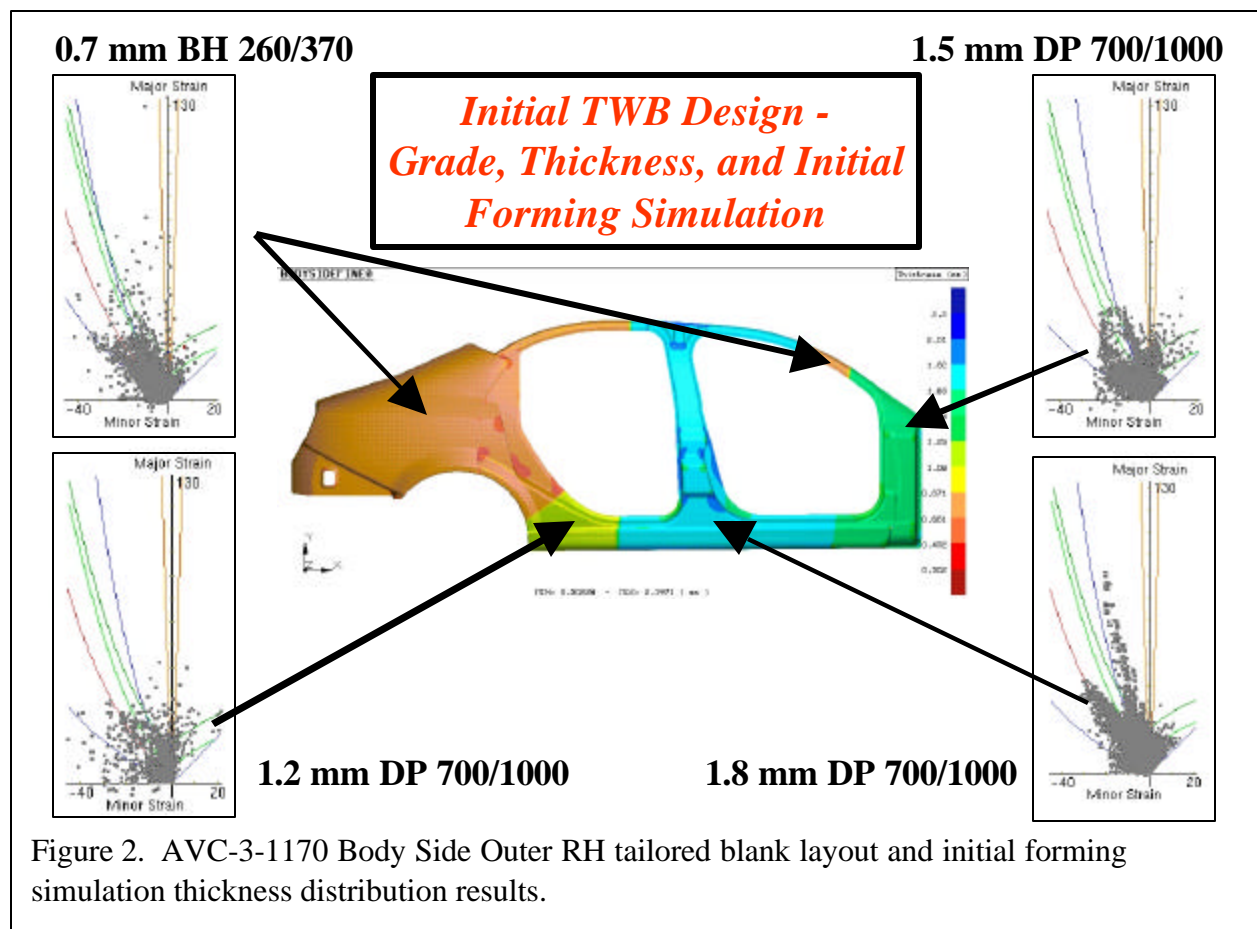
1. AVC-2-1016 Floor Front RH

The Floor Front is an example of an initial concept design with high forming strain safety margin that was selected for down-gauging to reduce mass. This PNGV class-specific component was originally estimated to require a 0.7 mm 220 MPa yield strength steel stamping. Initial forming simulations using 0.7 mm IS 220/300 stamping predicted all areas of the part would exhibit strains well below the forming limit. Forming simulations were repeated with successively higher strength, lower gauge grades until the predicted forming strains became critical. This process concluded that the Floor Front could be successfully stamped from 0.5 mm TRIP 400/700. Forming simulation results for both the 0.7 mm IS 220/300 and 0.5 mm TRIP 400/700 are shown in Figure 1. Following a review of their concept design calculations, and based on their experience with NVH considerations, PES determined the part could be reduced in gauge from 0.7 to 0.65 mm without compromising structural performance and crashworthiness. PES selected TRIP 450/800 for the lighter gauge application. This gauge change reduced left- and right-hand part mass by 7% and removed 0.636 Kg from the body structure.

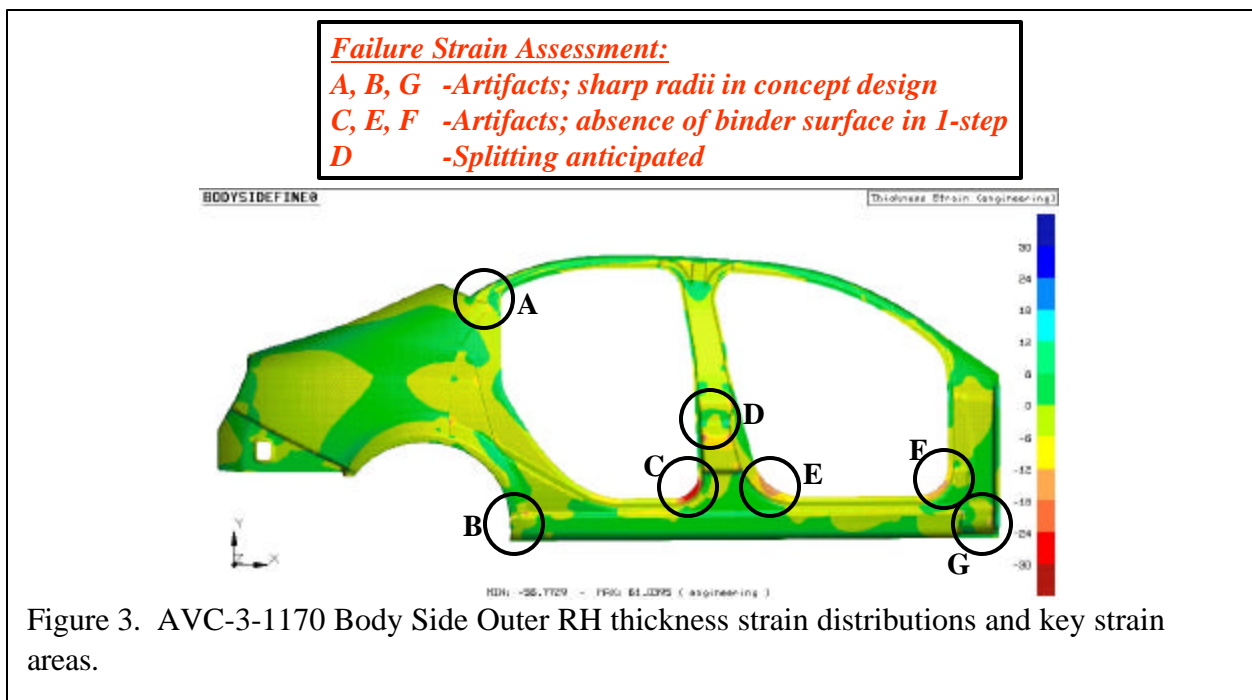


2. AVC-3-1170 Body Side Outer RH

The Body Side Outer exemplifies how FEA forming simulation was used to recommend geometry and grade changes to assure forming feasibility in a large, complicated tailored blank stamping. The initial PES concept design for this component was a 5-piece tailored blank to be stamped from 0.7 mm BH 260/370 for the exposed rear fender and unexposed forward roof rail; 1.2 mm DP 700/1000 for the fender to lower rocker transition; 1.8 mm DP 700/1000 for the B-pillar; and 1.5 mm DP 700/1000 for the A-pillar. The tailored blank layout (gauge/grade locations) and initial forming simulation results (thickness distribution) are shown in Figure 2.

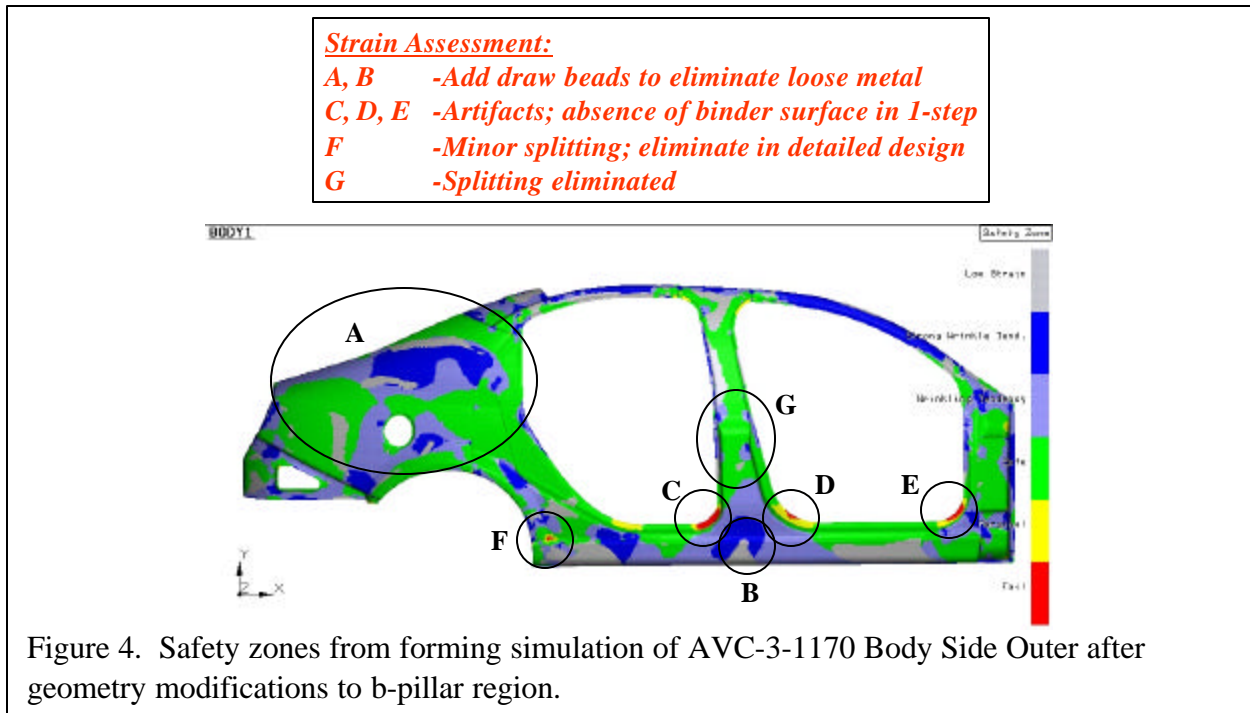


The thickness strain distributions predicted by the initial simulations are illustrated in Figure 3 and highlight key areas with predicted failure strains. Failure strains at areas A, B, and G in Figure 3 are sharp features to which radii were not added in the concept design. Since ULSAB-AVC is a concept design, it is, of course, beyond the project's scope to blend all corners as would be done in a detailed design phase. These strains were not considered significant and were ignored, since strains in these locations can be made safe by adding full design details if necessary. Similarly, the failure strains at locations C, E, and F in Figure 3 are one-step were ignored because they are simulation artifacts resulting from the absence of a binder surface on the part blank; adding the full binder surface in a detail design phase would eliminate these problem strains. Failure strains in area D at the lower portion of the B-pillar, however, were considered significant and geometry modifications were recommended to reduce strains.



PES designers took the Body Side Outer forming simulation results into consideration when optimizing the concept design and made appropriate changes to lower B-pillar geometry to alleviate failure strains. The safety zones predicted by the forming simulation of the modified part are shown in Figure 4, which highlights the key strain features.

Areas A and B in Figure 4 represent areas of loose metal that can be eliminated by the addition of blank holder force in a detailed design phase prior to die development. Failure strains in areas C, D, and E in Figure 4 are, again, artifacts of the one-step forming simulation method that resulted from the absence of binder surface in the door cut-out area and should disappear when the binder is added.



Significant failure strains, however, persist in area F but should be alleviated by detailed design and die development work. Strains in area G are now safe following the geometry modification.

While the geometry modification eliminated failure strains in the B-pillar, concern remains about the high strains in the plan view radii at the bottom of the A- and B-pillars (circled as areas C, D, and E in Figure 4). If the addition of a binder surface to the door opening cut-out does not completely relieve strain in this area, adding a drawbead to the external binder surface to pull out the low strain area in the rocker below the B-pillar could increase strain at the plan view radii and splitting may return.

An additional simulation was conducted, in which 1.8 mm DP 500/800 was substituted for DP 700/1000 in the B-pillar area. This simulation indicated that all strains in the B-pillar remain below the forming limit, except for the failure strain artifacts at the cut edge of the part at the plan view radii below the A- and B-pillars. Forming strains in the lower portion of the B-pillar are sufficient to strain plus age harden the DP 500/800 to a final yield strength of 700 MPa.

Strains in the upper portion of the B-pillar could be increased to similar levels by the addition of binder force or drawbeads. Should this part enter detailed design and die development, and if detailed design and die development modifications did not eliminate low strain in the rocker below the B-pillar, the part could potentially be made without increasing mass by substituting 1.8 DP 500/800 in the B-pillar areas and using strain plus bake hardening to increase yield strength to 700 MPa.

Dies for stamping tailored blanks normally contain steps in the binder surface to accommodate the change in thickness across the weld line when multiple gauges are employed. Metal movement in the die during stamping must be controlled to limit movement in the vicinity of the weld to a direction parallel to the weld line to 1.) prevent heavier gauge material from moving into the smaller binder gap area and 2.) prevent scoring of the die surface by transverse movement of the weld step. Metal flow during stamping of the PNGV-class body side outer was evaluated with the aid of the x- and y-metal movement plots shown in Figures 5 and 6,

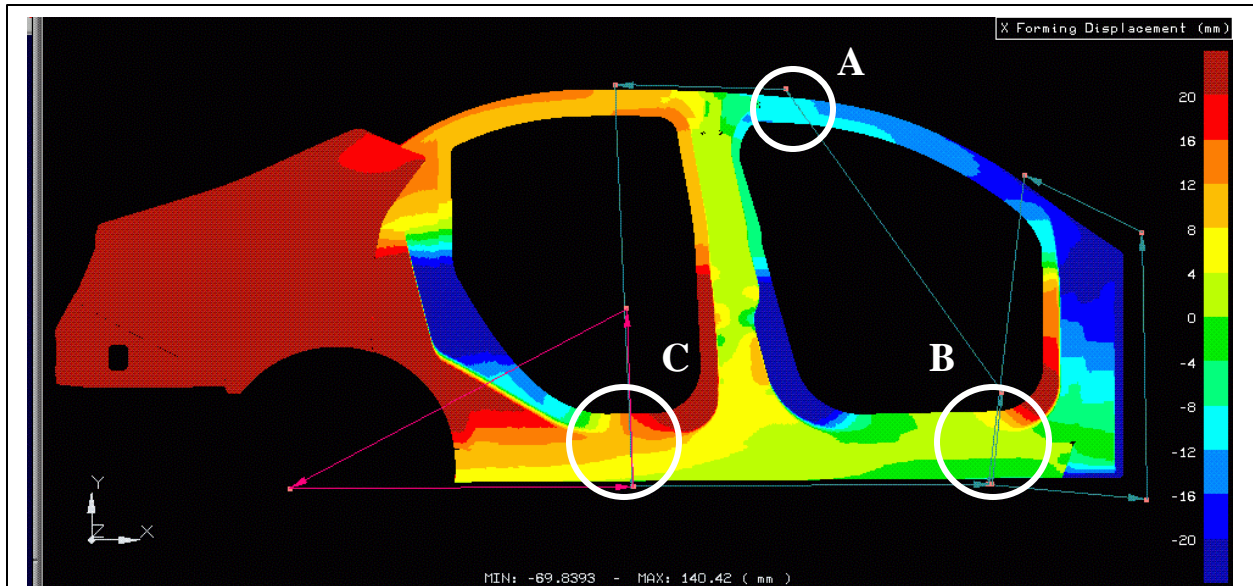


Figure 5. Map of x-direction metal movement in ULSAB-AVC PNGV-class body side outer tailored blank stamping (positive x-direction is horizontal to the right). Excessive transverse weld line movement is noted at areas marked A, B, and C.

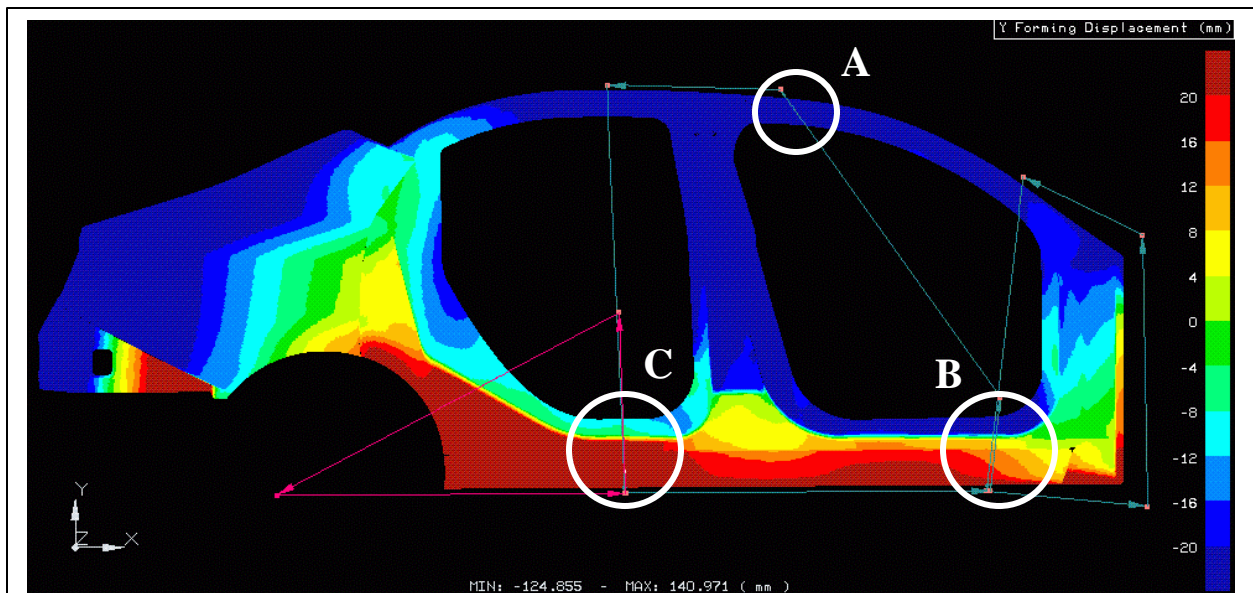


Figure 6. Map of y-direction metal movement in ULSAB-AVC PNGV-class body side outer tailored blank stamping (positive y-direction is vertical upward). Excessive transverse weld line movement is noted at areas marked A, B, and C.

respectively. Excessive transverse weld line movement was noted in areas marked A, B, and C in these figures.

Excessive transverse movement at area A (32 mm) can be reduced by rotating the weld line direction clockwise to align it with the direction of metal flow, which is downward and to the rear of the blank. Excessive transverse movement at area B (21 mm) can be reduced by moving the position of the weld slightly rearward to place it in an area of smaller x-direction strain. Excessive transverse movement at area C (22 mm) can be reduced by moving the weld slightly to the rear and rotating it clockwise to place the weld in an area of lower x-direction strain and orient it closer to the direction of major metal flow. Each of these changes are modifications that would normally be made in the detailed design phase and should be feasible.

4. AVC-2-1069 Floor Rear

The Floor Rear is another example of forming simulation performed for a large tailored blank stamping. This C class-specific component was initially designed as a four-piece tailored blank stamping. PES selected 0.6 mm BH 210/340 for the center portion, 1.5 mm DP 350/600 for the two longitudinal side portions, and 0.7 mm DP 700/1000 for the transverse portion at the rear of the blank. The part is symmetrical and the forming simulation considered only one half.

The layout of the tailored blank (grade and gauge locations) and results of the forming simulation (thickness distribution) for the C-class Floor Rear tailored blank stamping are shown in Figure 7. Strains in the 1.5 mm DP 350/600 portion are largely below the forming limit, and strains in the 0.6 BH 210/340 portion are all well below the forming limit. The 07 mm DP 700/100 portion contains some failure strains.

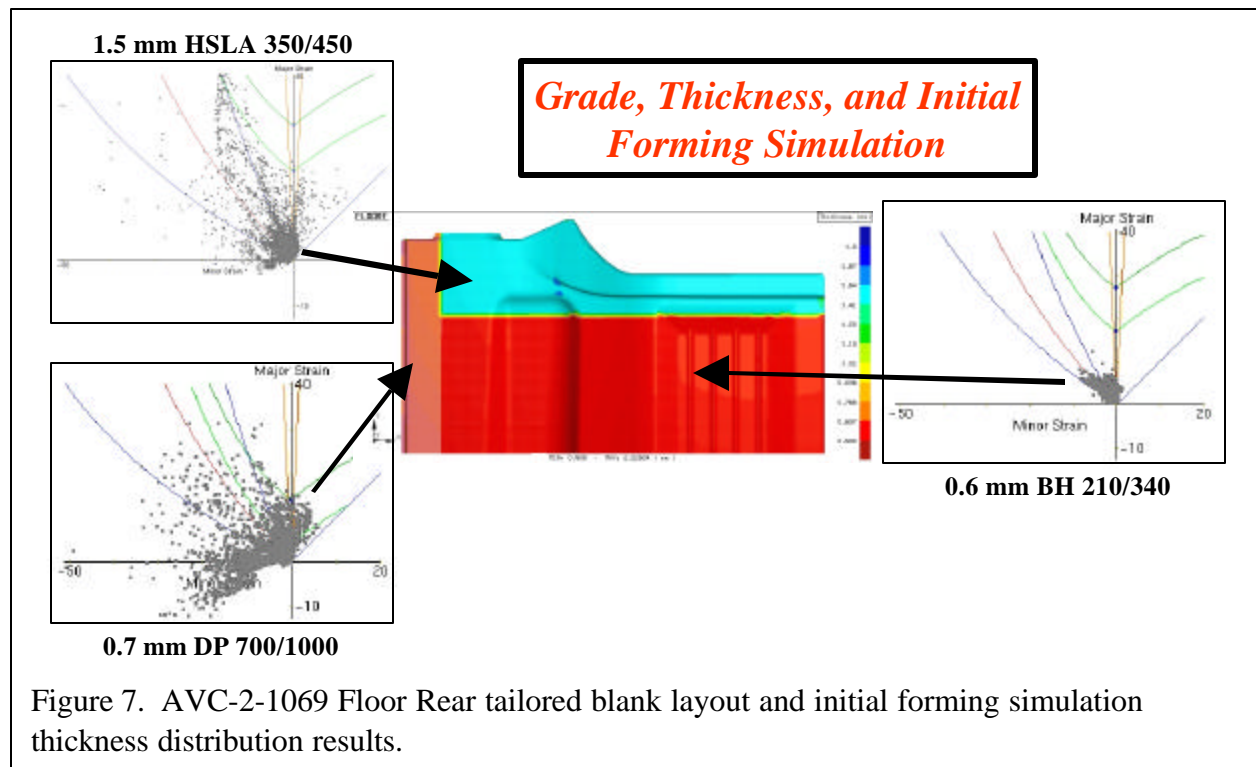


Figure 7. AVC-2-1069 Floor Rear tailored blank layout and initial forming simulation thickness distribution results.

The thickness strains predicted for the Floor Rear forming simulation are shown in Figure 8, which highlights several key forming strain areas. Failure strains at A and B were considered to result from the absence of radii and would be eliminated in a detailed design phase. The failure at area C is due to a combination of sharp radius and excess strain during flanging. The addition of a cutout would eliminate the failure strain. Failure at area D is caused by excess strain during flanging and can be eliminated by deepening an existing cutout.

PES designers considered the forming simulation results during concept design optimization and determined on the basis of structural and crashworthiness assessments that the gauge of the 1.5 mm DP 350/600 portions of the blank could be reduced to 1.1 mm. The final concept design utilizes this gauge and grade in the longitudinal side portions of the part. This gauge reduction reduced part mass by 1.736 Kg or 12%.

